UNIVERSITY OF CALIFORNIA, SAN DIEGO

Cooperative motions in supercooled liquids and glasses

A dissertation submitted in partial satisfaction of the
requirements for the degree
Doctor of Philosophy

in

Physics

by

Jacob D. Stevenson

Committee in charge:

Professor Peter G. Wolynes, Chair
Professor Katja Lindenberg
Professor Lu Sham
Professor Sinul Sinha
Professor Michael Tauber

2009

The dissertation of Jacob D. Stevenson is approved, and it is acceptable in quality and form for publication on microfilm:

_____

_____

_____

_____

_____

Chair

University of California, San Diego

2009

TABLE OF CONTENTS

LIST OF FIGURES

LIST OF TABLES

ACKNOWLEDGEMENTS

I would like to thank my thesis adviser, Peter Wolynes, for all his help and support through the years. His guidance, inspiration, and motivation have helped me immeasurably. I would also like to thank my parents, my sisters, and especially my amazing wife Tara. Her patience and support has never wavered and has always been appreciated.

Chapter 2, in full, is a reprint of the material as it appears in the Journal of Physical Chemistry B 109 15093–15097 (2005), J. D. Stevenson and P. G. Wolynes. The dissertation author was the primary investigator and author of this paper.

Chapter 3, in full, is a reprint of the material as it appears in Nature Physics 2 268–274 (2006), J. D. Stevenson, J. Schmalian, and P. G. Wolynes. The dissertation author was the primary investigator and author of this paper.

Chapter 5, in full, is a reprint of the material as it appears in the Journal of Chemical Physics 129 194505 (2008), J. D. Stevenson, A. M. Walczak, R. Hall, and P. G. Wolynes. The dissertation author was the primary investigator and author of this paper.

Chapter 6, in full, is a reprint of the material as it appears in the Journal of Chemical Physics 129 234514 (2008), J. D. Stevenson and P. G. Wolynes. The dissertation author was the primary investigator and author of this paper.

VITA

2003	Bachelor of Arts in Physics and Mathematics *cum laude*, Cornell University, Ithaca, NY
2003-2004	Graduate Teaching Assistant, University of California, San Diego
2004-2009	Graduate Researcher, University of California, San Diego
2005	Master of Physics, University of California, San Diego
2009	Doctor of Physics, University of California, San Diego

PUBLICATIONS

J. D. Stevenson and P. G. Wolynes, "On the surface of glasses. *J. Chem. Phys.* 129, 234514 (2008).

J. D. Stevenson, A. M. Walczak, R. W. Hall and P. G. Wolynes, "Constructing explicit magnetic analogies for the dynamics of glass forming liquids." *J. Chem. Phys.* 129, 194505 (2008).

J. D. Stevenson, J. Schmalian and P. G. Wolynes, "The shapes of cooperatively rearranging regions in glass-forming liquids." *Nature Physics* 2, 268274 (2006).

J. D. Stevenson and P. G. Wolynes, "Thermodynamic-kinetic correlations in supercooled liquids: A critical survey of experimental data and predictions of the random first-order transition theory of glasses." *J. Phys. Chem. B* 109, 1509315097 (2005).

ABSTRACT OF THE DISSERTATION

Cooperative motions in supercooled liquids and glasses

by

Jacob D. Stevenson
Doctor of Philosophy in Physics
University of California San Diego, 2009
Professor Peter G. Wolynes, Chair

Why glasses behave like solids in the absence of their having any long range structural order, is a fundamental problem of statistical physics, one that has been actively researched for more than 80 years. Supported by the mean field theory of supercooled liquids and a deep connection to mean field spin glasses with one step replica symmetry breaking, the random first order transition theory offers a solution to the glass problem based on assuming proximity to an underlying ideal glass transition. In the deeply supercooled liquid the free energy landscape is dominated by metastable structural basins separated by large free energy barriers. The rate of inter-conversion between these structural states is ultimately driven by the entropic cost of remaining confined to one basin, a cost which is quantified by the configurational entropy. Both the activation free energy barrier and the number of cooperatively moving particles required to overcome the barrier diverge as the ideal glass transition is approached. The cooperative nature of the dynamics in the deeply supercooled liquid regime has been confirmed by experiments and simulations and has been the subject of intense study in recent years. In the following we explore the implications of cooperative dynamics in the random first order transition theory with particular focus on the expected behavior at the ideal glass transition temperature and at the dynamical crossover, the temperature where activated motions first become important. We also show how the general features of secondary relaxation can be recovered by adding local fluctu-

ations to the equations describing cooperative reconfiguration. Finally, we describe how cooperatively rearranging regions modify dynamics near the surface of glasses, reducing the apparent viscosity by several orders of magnitude.

Chapter 1

Introduction

The fundamental issue underlying all the questions surrounding the glass transition is to understand why glasses behave like a solid. The rigidity does not come from an ordering of the molecules. Rather the viscosity increases continuously to the point it becomes unmeasurably long. The increase in viscosity is often so rapid that neither a power law, nor Arrhenius behavior are sufficient descriptors, and, in fact the increase is so rapid that it is difficult to describe without acknowledging that it appears to diverge at a finite temperature. The functional form most often used to fit the data, the Vogel-Tammann-Fulcher (VTF) equation $\eta = \eta_0 \exp(B/(T - T_0))$ reflects this, including an explicit divergence of the viscosity at temperature T_0. This apparent finite temperature divergence motivates the concept of an underlying ideal glass transition: an ergodicity breaking thermodynamic phase transition. Strengthening this notion is the impending problem of an entropy crisis first noticed by Simon[2] and highlighted by Kauzmann[3] in 1948. In the experimentally accessible regime $T > T_g$ the liquid entropy decreases rapidly. Extrapolating below T_g, the liquid entropy would appear to become smaller than that of the crystal at a temperature T_K, and even would appear to vanish or become negative at a non-zero temperature in violation of the third law of thermodynamics. In practice the rapidly increasing relaxation time means the system always falls out of equilibrium before anything untoward happens. In principle an experiment conducted with infinite patience must see some resolution to

the entropy crisis, and a candidate theory of glassy behavior must either account for such a vanishing entropy or show how the crisis is avoided. Subtracting the vibrational entropy of the crystal from the liquid entropy leaves to a good approximation the configurational entropy S_c associated with the structural degeneracy of the non-crystalline arrangement of molecules. One theoretical strategy relates the vanishing of this configurational entropy to the ideal glass transition, a notion that is strongly supported by the remarkable agreement between the Kauzmann temperature, where s_c vanishes, and the VTF temperature, where the viscosity diverges. As is demonstrated in figure 1.1 the two agree to within a few percent for a wide assortment of materials[4]. Adam and Gibbs[5] were among the first to construct a theory in which the vanishing configurational entropy would drives the increasing viscosity. They proposed that molecular motion occurs cooperatively with an activation barrier proportional to the volume of the mobile region, and inversely proportional to the configurational entropy yielding their eponymous relation $\eta = \eta_0 \exp(A/S_c(T))$. This relation, which recovers the VTF equation for $T_K = T_0$, along with the concept of cooperatively rearranging regions (CRR) has had tremendous influence on the field.

Laying the ground work for a more rigorous understanding of glassy behavior were two intimately connected theories, the mean field theory of structural glasses and mode coupling theory. Mean field studies of amorphous structural packings have demonstrated that configurational states first become metastable below some critical temperature[6, 7]. In this picture the free energy landscape breaks up into metastable basins separated by activation barriers. In mean field all barriers are proportional to the system size and therefore infinite in the thermodynamic limit. Mean field predicts the breaking of ergodicity at this temperature. Of course in real systems metastable states are truly metastable, and activated hopping between basins smooths the transition and restores ergodicity. The mode coupling theory (MCT)[8, 9] of the glass transition was an early and partially successful theory which derived dynamical equations from microscopic arguments. This theory accurately describes the evolution of the density auto-correlation function as it abandons simple exponential decay and develops a plateau. The resolution involves a separation of time scales into rapid local decay to the plateau, corresponding to molecules vibrating within their structural cages, and slow large scale motions corresponding to restructuring of the

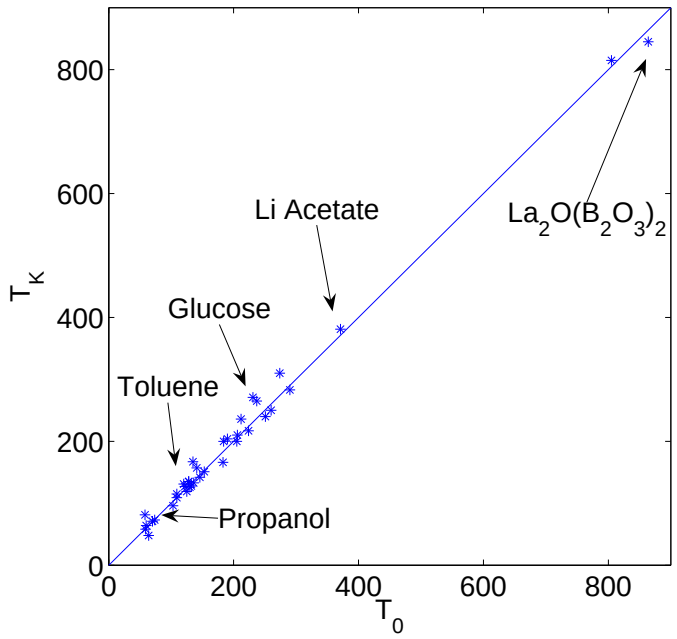

Figure 1.1: The extrapolated temperatures of the vanishing configurational entropy at T_K and diverging viscosity T_0 agree for a wide array of materials. Data taken from reference [4].

cages themselves. Mode coupling theory even predicts a "glass transition" of sorts, as the long time scale diverges at a temperature T_A. However, neither the value of T_A (the predicted divergence occurs far above the laboratory glass transition) nor the prediction of a power law divergence is realized. Instead it was shown that this mode coupling temperature coincides with the emergence of metastable structural configurations[10] and that mode coupling theory is itself a mean field theory, the prediction of broken ergodicity being the mean field artifact of infinite activation barriers. Despite its failings, MCT is generally seen as correctly describing the onset of glassy behavior and as such is often been used as a touchstone for theoretical approaches.

These scattered features and theoretical approaches of supercooled liquids began to coalesce under a single theoretical umbrella when the deep similarities between the phase

space of the Potts and p-spin glass models and the emerging picture of structural glasses was pointed out[10]. In mean field the p-spin glass can be solved exactly[11, 12, 13] and displays a confusing asymmetry between statics and dynamics. The thermodynamic solution shows a static transition at T_s, while the dynamical equations show that time scales diverge and ergodicity is broken at $T_d > T_s$. The resolution to this quandary is the existence of metastable states, which first emerge below the dynamic transition. The broken ergodicity in the dynamic equations reflect the fact that metastable states are separated by infinite free energy barriers in mean field. On the other hand for $T > T_s$ metastable states have negligible thermodynamic weight with respect to the paramagnetic phase and are therefore invisible in the thermodynamic calculation. The configurational entropy, the log of the number of metastable states, vanishes at T_s where the number of states becomes sub-exponential. In mean field systems metastable states have infinite barriers and ergodicity is broken below T_d, in finite range systems the transition at T_d becomes merely a dynamic crossover and the relaxation time remains finite until T_s. The similarities between the p-spin glass and structural glass are plentiful and obvious. With the identification of T_A with T_d and T_K and T_0 with T_s the following picture emerges

$T \gg T_A$: The p-spin glass is in the paramagnetic phase and equilibrates rapidly. The supercooled liquid relaxes rapidly via diffusion.

$T \gtrsim T_A$: The dynamics of both systems are described by the equations of mode coupling theory. As the relaxation times increase the the auto-correlation functions of both systems develop a plateau implying the systems remains in finite regions of phase space for extended periods of time.

$T \to T_A^+$: In mean field the plateaus and therefore the relaxation times diverge, breaking ergodicity.

$T_K < T < T_A$: Metastable states emerge below T_A and correspond to locally stable configurations of molecules (spins). The number of metastable states is exponentially large and decreases with decreasing temperature. In finite dimensions transitions between metastable states have finite barriers, which grow with decreasing temperature and

increasingly dominate the dynamics.

$T \to T_K$: The number of states becomes sub-exponential (the configurational entropy per particle vanishes), but the lowest energy states achieve statistically significant weight. Free energy barriers diverge and ergodicity is broken. T_K signals a true thermodynamic phase transition with aspects of a second order transition (continuous in the volume, energy, and entropy, and discontinuous in the heat capacity and other susceptibilities), but on the other hand is discontinuous in the relevant order parameter, a signal of a first order transition. Possible order parameters include the infinite time limit of the density auto-correlation function or the replica overlap. This unusual phase transition is called "random first order."

The mean field dynamic divergence of supercooled liquids at T_A described by mode coupling theory signals the emergence of metastable states, and becomes a dynamic crossover in finite range systems[10, 14, 6, 7]. Below T_A the system can become trapped in metastable configurations for extended periods of time, and activated barrier hopping becomes the primary means of transport. The calculation of viscosity is reduced to finding the free energy barriers to reconfiguration. Consider a liquid prepared in metastable state α a region of which (of linear extent r) has transitioned to a new metastable state β. As at an ordinary first order transition there is imperfect energy minimization at the interface resulting in a free energy penalty $\sigma_{\alpha\beta} r^\theta$, but in contrast to ordinary first order transition the two states have roughly the same energy. The nucleated region is unstable for all values of r. Now consider the situation where the destination state β is left unspecified. In this case the nucleated droplet gains the entropy associated with the number of possible metastable states. Since the number of available states is exponential in the system size, this term is proportional to $TS_c r^3$. The difference in free energy between the final state and the initial state is

$$\Delta F(r,T) = -\frac{4\pi}{3} T S_c r^3 + 4\pi\sigma_0 r_0^2 (r/r_0)^\theta. \tag{1.1}$$

The droplet interface energy of disordered systems typically scales with exponent θ less than the natural value of 2. For supercooled liquids, the correct value of the exponent has

been much discussed[15, 16, 17, 18], and while it has not been experimentally determined, renormalization group arguments have suggested that it should be $\theta = 3/2$[19, 20]. The typical value of the mismatch coefficient is estimated using density functional theory[6, 21] to be $\sigma_0 = 3/4 k_B T r_0^{-2} \ln[1/(d_l^2 \pi e)]$. The Lindemann length d_l, the magnitude of molecular vibrations required to break up a frozen crystal structure, is close to $d_l = 0.1$ inter-particle spacings (r_0) for many substances and leads to the remarkable universality of glassy behavior.

The free energy profile of equation 1.1 demonstrates that a system prepared in a single metastable state is unstable to droplet fluctuations and will be broken up into regions of size no smaller than

$$r^* = r_0 \left(\frac{3\sigma_0}{r_0 T S_c} \right)^{1/(3-\theta)} \tag{1.2}$$

This activated process of droplet dynamics destroys the quasi-order of a single metastable state solution and smooths out the mean field divergences of mode coupling theory and is what dominates the dynamics in the temperature region $T_K < T < T_A$. The time scale of this process has been shown to be dominated by the bottleneck in the droplet growth[22, 21]. Thus the time scale of droplet dynamics, the primary mechanism of α relaxation, is $\tau_\alpha = \tau_0 \exp(F^\ddagger / k_B T)$ where the free energy barrier is given by

$$F^\ddagger = 4\pi(1-\theta/3)(\sigma_0 r_0^2)^{\frac{3}{3-\theta}} \left(\frac{\theta}{r_0^3 T S_c} \right)^{\frac{\theta}{3-\theta}} \quad \xrightarrow{\theta=3/2} \quad \frac{3\pi\sigma_0^2 r_0}{T S_c}. \tag{1.3}$$

The concepts sketched above form the framework of the random first order transition theory (RFOT) and describe how the dynamics of supercooled liquids, governed by the mode coupling equations at high temperatures, give way to entropically driven, activated reconfiguration events below the dynamical crossover temperature. These events are necessarily cooperative and take place on a length scale r^* given by equation 1.2. This length scale and the associated relaxation time are universal functions of the configurational entropy. The length scale is about five inter-particle spacings at the glass transition temperature. The predictions of both the magnitude and universality of the cooperatively rearranging regions have recently been validated[23, 16] as is shown in figure 1.2. The length and time

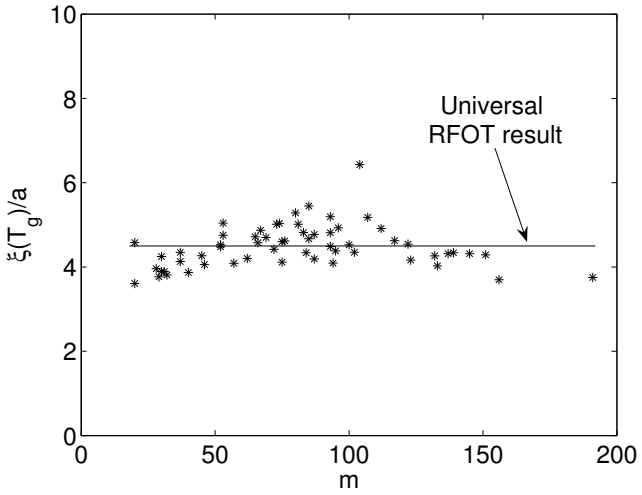

Figure 1.2: **Dynamical correlation lengths** determined from the Berthier et al. relation[23] $\xi(T_g)/a = \left(\frac{\log(10)^2}{\pi e^2}\beta^2 m^2 k_B/\Delta C_P\right)^{1/3}$. The values of ΔC_P were found using the relation $m = 20.7\Delta C_P/k_B$, where ΔC_P is given per independently rearranging molecular unit, or "bead"[24]. All data were taken from Böhmer et al.[25]

scales both increase with decreasing temperature and approach a divergence at the ideal glass transition temperature T_K. The foundation having been laid for the understanding of the dynamics of supercooled liquids, in the following I explore in this thesis some of the myriad implications of the cooperative nature of activated motion in supercooled liquids. I pay particular attention to the limits of the theory, the expected behavior at the ideal glass transition temperature and how the theory is modified near the dynamical crossover, the temperature where activated motion first becomes important.

Chapter 2 explores in detail the remarkable relationship between dynamics and thermodynamics of supercooled liquids. It is shown that the purely dynamic quantity fragility can be very accurately determined by the excess heat capacity, a purely thermodynamic quantity.

It is known that the length scale of cooperativity grows as the glass transition is approached, but there is conflicting evidence as to whether the cooperativity manifests itself as stringy, chain-like motion or as compact clusters of mobile particles. Chapter 3 accounts

for the entropic advantage of stringy clusters (there are many possible paths in constructing a string, but only one way to make a sphere) and show that in the deeply supercooled regime the dominant cooperative motion is likely to be compact, while at higher temperatures stringy chains are the preferred mode of relaxation. Within this model there exists a temperature where the free energy barrier for stringy motion vanishes. I identified this temperature as the crossover between the low temperature regime dominated by activated motion and the high temperature (mode coupling) regime dominated by collisional transport. Our theory for this temperature predicts a previously unnoticed correlation with the configurational heat capacity that agrees well with the experimentally measured dynamical crossover (mode coupling) temperatures.

Nearly all glass forming liquids display secondary relaxations, dynamical modes seemingly distinct from the primary alpha relaxations. It is shown in chapter 4 that accounting for driving force fluctuations and the diversity of reconfiguring shapes in the random first order transition theory yields a low free energy tail on the activation barrier distribution which shares many of the features ascribed to secondary relaxations. While primary relaxation takes place through activated events involving compact regions of the liquid, secondary relaxation corresponding to the tail is governed by more ramified, string-like, or percolation-like clusters of particles. These secondary relaxations merge with the primary relaxation peak and become dominant near the dynamical crossover temperature T_c, smoothing the transition between continuous dynamics described by mode-coupling theory above T_c and activated events below T_c.

Chapter 5 develops a mapping between the dynamics of supercooled liquids (specifically the process of escape from a free energy minimum corresponding to a locally metastable structural configuration) and an Ising model on a topologically disordered lattice. The parameters of the Ising system are determined from the instantaneous static structure of the glass via density functional theory and the replica overlap approach. This mapping is used to explore the scaling and fluctuations of droplet dynamics in a sampled Lennard-Jones glass. Renormalization group results for random magnets, when combined with the statistics for the Lennard-Jones glass, suggest that the ideal glass transition, identified by the Kauzmann temperature, is actually a true phase transition with diverging length and time

scales and characterized by discontinuous replica symmetry breaking.

Experiments over the past few decades have successfully shown that molecules near the surface of glasses exhibit much higher mobility than do molecules in the bulk glass. This was recently exploited to create highly stable glasses via vapor deposition in a series of experiments in the Ediger laboratory at the University of Wisconsin-Madison. To create glasses of the same structural stability that was achieved by vapor deposition via traditional cooling methods would require about ten thousand years. Chapter 6 discusses an idealized model describing how a free surface reduces the pinning field restraining the particles' motion. The model shows that activation barriers near a free surface are reduced by a factor of two with respect to the bulk, leading to the simple relationship between the relaxation times in the bulk and near the surface, $\tau_{surf} = \sqrt{\tau_0 \tau_{bulk}}$. It is also shown that this dramatic decrease in the relaxation time sets up a massive gradient in the mobility field which is spread out by the mechanisms of mode coupling theory. These calculations allow a prediction of the mobility profile as a function of the distance from the surface. The theoretical results agree with the available data and may soon be further tested by experiments currently being conducted to probe mobility as a function of depth.

Chapter 2

Thermodynamic—kinetic correlations in supercooled liquids: A critical survey of experimental data and predictions of the random first-order transition theory of glasses

The glass transition, as observed in the laboratory is a kinetic phenomenon. Unlike crystallization, the definition of the transition to the glassy state depends on experimental time scales. The change in mechanical response is accompanied by changes in thermal properties. Most dramatically the heat capacity drops upon cooling through the transition. This drop is quite measurable and generally appears to approach a discontinuity as the experimental time scale is increased. A variety of mean field models of disordered spin systems, electrical materials, and molecular fluids predict a true thermodynamic transition

with such a heat capacity discontinuity. In these models, the thermodynamic transition occurs at a temperature T_K, where the configurational entropy of different mean field solutions vanishes. [10, 14, 26, 19, 27, 28, 29, 30, 31, 32, 33, 34, 35] These mean field frozen configurations first appear discontinuously at a higher dynamical transition temperature T_A, which coincides with the mode coupling transition for these models. It is natural to take these mean field theories, even given their status as approximations, as the starting point to understand the laboratory glass transitions, as much as mean field theories are the natural starting point to understand critical phenomena [36, 37] and nucleation dynamics at ordinary first-order transitions. [38, 39] But they are only a starting point. Indeed, just as mean field theories of ordinary first-order transitions must be supplemented by Maxwells construction[40, 41] and by a theory of nucleation rates [42, 43] to describe how ordinary first-order transformations occur in the laboratory, the connection of the existing mean field theories with real supercooled liquids can be made only by constructing entropic droplets which smear out the pure dynamical transition at T_A and function as the mechanism of the slow α relaxation, which, when it falls out of equilibrium, characterizes glass formation. If the underlying entropy crisis at T_K remains in finite range systems (a debatable point), [44] then a dynamical theory based on entropic droplets yields a free energy barrier consistent with the commonly used Vogel-Fulcher law having a divergence at a temperature T_0, which according to this theory coincides with T_K.

$$\tau_\alpha = \tau_0 e^{DT_0/(T-T_0)} \tag{2.1}$$

While the well-known observed confluence of kinetic divergence at T_0 and the entropy crisis at T_K is based on extrapolation from the experimentally accessible time scales, and has thus been questioned, this confluence is naturally explained by random first-order transition (RFOT) theory. As Angell has often pointed out,[4] the empirical correlation between thermodynamics and kinetics goes much further than merely this confluence of T_0 and T_K. The further connection can be seen in the coefficients D. The coefficient, D, varies considerably from substance to substance. The key experimental finding is that the larger the observed heat capacity change, ΔC_p, at T_g, the smaller the D values. This has led to the concept of fragility of liquids which can be termed either "strong" or "fragile"

depending on their D values. Within the RFOT framework, understanding the observed thermodynamic/kinetic correlations over a wide range of substances requires a microscopic theory of the free energy cost of entropic droplets. This microscopic theory was provided by Xia and Wolynes,[21] who, using a density functional treatment of a glass transition of a fluid of spherical particles,[6] argued that near T_g this free energy cost depended both on the configurational entropy drive to form the droplets and on a free energy cost for mismatched areas, σ, which the density functional theory relates to the entropy cost of localizing the particles, $\sigma_0 = 3/4r_0^{-2}k_BT\log(\alpha/\pi e)$. The former terms dependence on temperature is reflected in Cp. The latter mismatch energy depends only logarithmically on the effective spring constant, α, characterizing the caging. α is the inverse-square amplitude of vibrational motions in a glassy configuration to the interparticle spacing and is related to the Lindemann ratio. The Lindemann ratio has been measured via neutron scattering and predicted by density functional theory. It varies only slightly from substance to substance, and α is found to be of order 100, the value we will use. Therefore the mismatch energy, which depends only logarithmically on this ratio, is predicted to be a nearly universal quantity in units of k_BT_g. In this way, as discussed in references [21] and [45], if the transition were an ordinary first-order one, then the free energy of a nucleating droplet would be given as a function of the radius of the droplet

$$F(r) = -\frac{4}{3}\pi T s_c r^3 + 4\pi\sigma r^2 \tag{2.2}$$

The critical value of r from this theory gives a reconfiguration barrier proportional to S_c^{-2}. For a random first-order transition there is a multiplicity of solutions that can "wet" the droplet. To account for this, RFOT theory uses an idea from Villain first worked out for the random field Ising model to estimate how much the interface is wetted by specific solutions that better match the original. This wetting lowers the mismatch energy, $\sigma(r) = \sigma_0(r_0/r)^{1/2}$, and leads to the free energy barrier scaling with $1/S_c$, $\Delta F^{\ddagger} = 3\pi\sigma_0^2 r_0/TS_c$. This wetting argument also restores the consistency of the critical exponents at T_K with hyperscaling. When the mismatch energy is combined with the Xia-Wolynes value of σ_0, it immediately follows that D and ΔC_p should be inversely related, as was generally observed.[46] Furthermore, the numerical coefficient of the mismatch energy

is predicted by the microscopic calculation, crude as it is in some respects, so that the specific relation $D = 32k_B/\Delta C_p$ follows from the Xia-Wolynes (XW) treatment and can be tested. It is important that this relation is predicted for spherical particles, and therefore the ΔC_p must refer to the heat capacity change for each of these spheres which might be called "beads". Glasses can be chemically complex. Many glasses are clearly mixtures of nearly spherical entities, such as $KCaNO_3$. In such cases, counting "beads" is trivial. In other cases, chemical intuition allows a reasonable mapping of the molecular shapes on to an aggregate of spherical objects, for example, o-terphenyl involves three fused benzene rings, so it can be thought of crudely as consisting of three "beads". With only modest ambiguity, structural chemical knowledge usually would allow the measured change in heat capacity per mole of many glassforming substances to be converted to a heat capacity change per "bead". In this way, Xia and Wolynes tested the predicted relationship $D = 32k_B/\Delta C_p$ for five substances, and the microscopically predicted correlation was shown to be reasonably accurate.

Wang and Angell[47] made a survey of 44 substances with an eye to establishing quantitative relations between their thermodynamic and kinetic properties on a purely empirical basis without involving any microscopic theory. Their analysis deftly avoids entirely the question of bead count. They found an excellent correlation between, on the kinetic side, the so-called m values of the liquids, characterizing their activation energies at T_g and, on the thermodynamic side, ΔC_p (measured per mole), the glass transition temperature, T_g, and the latent heat of fusion per mole, ΔH_m. The m value is related to the D value described above; in fact, m is essentially the activation energy at the laboratory T_g in units of $k_B T_g$.

$$m = \left.\frac{\partial \log_{10} \tau}{\partial (T_g/T)}\right|_{T=T_g} \tag{2.3}$$

The empirical relation found by Wang and Angell is

$$m = 56 \frac{T_g \Delta C_p}{\Delta H_m} \tag{2.4}$$

At first sight, it appears strange that this relation should include the latent heat

of freezing, since, after all, the freezing transition is bypassed, strictly speaking, when a liquid supercools.

Lubchenko and Wolynes[45] suggested a theoretical route to a correlation of this form by using the same density functional style argument to characterize crystallization as was used to characterize vitrification by Xia and Wolynes. If each "bead" of a molecular fluid becomes fully localized in a three dimensional sense in the crystal, then the entropy of fusion per mole should be roughly the bead count per mole times the standard entropy of fusion of a spherical Lennard-Jones system. (Clearly this is an approximate relation since the small density change on freezing depends on details of the attractive forces which will vary from substance to substance.) Thus we can write

$$N_{\text{bead}} = \frac{\Delta H_m}{T_m} \frac{1}{S_{LJ}} \tag{2.5}$$

The entropy of fusion of Lennard-Jones spheres, per particle, S_{LJ} is $1.68k_B$.[45] When this relation is combined with the microscopic Xia-Wolynes prediction for $\Delta F^{\ddagger}$, and the well-known form of S_c, $S_c = S_\infty(1 - T_K/T)$ with S_∞ given by $\Delta C_p(T_g)T_g/T_K$, one obtains the result

$$m = \frac{T_m}{\Delta H_m} \Delta C_p \left\{ \frac{32 S_{LJ} \log_{10} e}{S_c^2(T_g)} \right\} \tag{2.6}$$

The residual entropy per bead at T_g is predicted by the Xia- Wolynes theory also to be universal,[45] $S_c(T_g) = 0.82k_B$. Thus, Lubchenko and Wolynes predicted the correlation

$$m = 34.7 \frac{T_m}{\Delta H_m} \Delta C_p \tag{2.7}$$

While resembling Wang and Angells correlation, strictly speaking, this prediction differs in form from the empirical correlation they introduced by containing the melting temperature in addition to glass transition temperature. Yet, a commonly used empirical rule for simple substances is that $T_m = 3/2T_g$. If this empirical relation is deemed to also hold, then Lubchenko and Wolynes pointed out that the Wang-Angell correlation is to be expected on the basis of the RFOT theory but with a theoretically predicted slope of 52, in contrast to the empirical slope of 56.

Table 2.1: A Survey of Experimental Data and Theoretical Results for 44 Materials. Includes an explicit calculation of m(theory) predicted by RFOT and the number of beads per molecule for each substance, predicted from the melting entropy.

materials	T_g (K)	m_{exp}	m_{theory}	T_m/T_g	ΔC_p $(J/Kmol)$	ΔH_m (kJ/mol)	T_m (K)	no. of beads	references
GeO2	810	20	17.7	1.71	6.27	17.1	1388	0.9	[25]
BeF2	590	24	18.0	1.40	3	4.76	825	0.4	[25, 48]
ZnCl2	380	30	27.4	1.56	13.7	10.24	591	1.2	[4]
methanol	106	34	45.5	1.65	24.4	3.26	175	1.3	[49, 50, 51]
n-propanol	96.2	40	39.7	1.55	41.5	5.4	148.8	2.6	[52, 53]
butyronitrile	97	47	44.5	1.66	39.87	5.02	161.4	2.2	[54]
Mg65Y10Cu25	402	49	47.1	1.82	16.1	8.65	730	0.8	[55]
ethylene glycol (ethanediol)	152.7	52	45.7	1.71	60	11.86	260.5	3.3	[53, 56]
ethanol	97	55	41.2	1.64	37.3	5	159	2.3	[53, 57]
m-xylene	125.5	56	48.7	1.80	72	11.56	225.3	3.7	[58]
glycerol	190	53	49.9	1.53	90.5	18.3	291	4.5	[59]
3-bromopentane	107	53	51.1	1.56	74	8.4	167.3	3.6	[53, 56, 60]
Pd40Ni40P20	570	55	54.0	1.55	16.54	9.39	884	0.8	[61, 62]
m-cresol	198.6	57	50.5	1.44	54	10.57	285	2.7	[58]
2-methypentane	78	58	55.2	1.53	83.4	6.26	118.3	3.8	[63]

Table 2.1: (continued)

materials	T_g (K)	m_{exp}	m_{theory}	T_m/T_g	ΔC_p $(J/Kmol)$	ΔH_m (kJ/mol)	T_m (K)	no. of beads	references
toluene	117	59	59.6	1.52	64	6.64	178.15	2.7	[53, 64]
fructose	286	61	53.8	1.32	133	32.43	378	6.1	[65, 66, 67]
phenolphthalein	363	62	57.3	1.47	146	47.15	533.7	6.3	[66, 68]
indomethacin	315	64	53.1	1.38	139	39.4	434	6.5	[69]
2-methylterahydrofuran	91	65	51.2	1.53	72	6.77	138.8	3.5	[25, 53, 60, 70, 71]
hydrochlorothiazide	385	65	56.5	1.42	92.3	31	547	4.1	[72, 73, 74]
griseofulvin	364	65	57.7	1.36	127	37.75	494	5.5	[72, 73, 74]
trinaphthylbenzene	337	66	60.3	1.41	122	33.3	474	5.0	[75, 76, 77]
di-2-ethylhexylphthalate	187	67	60.4	1.44	116	18	270	4.8	[78]
probucol	295	67	54.2	1.35	139.5	35.66	399	6.4	[72]
9-bromophenanthrene	224.75	69	63.1	1.48	76.5	14	333	3.0	[79]
phenobarbital	319	70	59.5	1.40	106.8	27.9	448	4.5	[72, 73, 74]
D-glucose	306	72	57.4	1.37	128	32.4	419	5.5	[4, 51, 65, 67]
glibenclamide	331	75	65.1	1.36	222.3	53.35	450	8.5	[72, 73, 74]
maltitol	311	94	64.5	1.35	243.6	55	420	9.4	[80, 81, 82]
salol	220	76	67.0	1.43	118.3	19.3	315	4.4	[59]
m-toluidine	187	79	66.9	1.33	168	8.8	249.5	2.5	[4, 58, 83, 84]
OTP	246	81	73.9	1.34	111.27	17.2	329	3.7	[59]
flopropione	335	81	68.7	1.35	127.5	29.1	452	4.6	[72, 73, 74]

Table 2.1: (continued)

materials	T_g (K)	m_{exp}	m_{theory}	T_m/T_g	ΔC_p $(J/Kmol)$	ΔH_m (kJ/mol)	T_m (K)	no. of beads	references
R-phenyl-cresol	220	83	58.7	1.49	120	23.3	328.2	5.1	[85]
selenium	308	87	40.4	1.60	14.4	6.12	494.33	0.9	[48, 53]
triphenylethene	248	91	69.8	1.38	120	20.35	341	4.3	[78, 86, 87]
sorbitol (D-glucitol)	266	93	85.3	1.44	189.45	29.5	383	5.5	[25, 4, 69, 81, 88]
H2SO43H2O	158	95	61.1	1.50	180	24.22	236.8	7.3	[48, 78, 89]
sucrose	323	97	98.1	1.44	250	41.1	465	6.3	[65, 66, 69]
Ca(NO3)24H2O	217	98	95.5	1.46	270.5	31.17	317	7.0	[48]
propylene carbonate (PC)	159.54	99	73.6	1.37	75.4	7.77	218.6	2.5	[90, 91]
TPP	200	104	63.9	1.49	155	25	297	6.0	[66, 69]
decalin	138.42	145	54.0	1.66	64	9.46	230	2.9	[92]

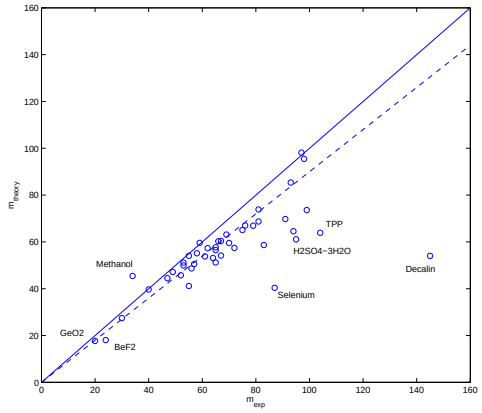

Figure 2.1: A plot of the fragility, m, measured from the experimental vs. the theoretical estimate derived from the random first-order transition theory. The solid line plots the perfect match, $m_{\rm exp} = m_{\rm theory}$; the dotted line, with slope 0.9, gives the best fit. The experimental data used are in Table 2.1 and are found in reference [47].

In this paper, we check the predicted Lubchenko-Wolynes relation[45] directly without assuming $T_m/T_g = 3/2$. Thus no empirical relation between T_m and T_g is invoked in the present analysis. The melting characteristics come in only as a way of relating the entropy costs of localizing real molecules that are not spherical to their locations in the crystal and the entropy loss for localizing "beads" which are assumed to be spheres, as envisioned by Lubchenko and Wolynes. A list of the substances and their properties is provided in Table 2.1. The data were kindly provided to us by Angell and are supplementary material to the Wang-Angell paper.[47] Notice the effective bead counts differ from the nearest integer by typically $10-20\%$. This reflects the approximate nature of the mapping. Figure 2.1 plots the measured $m_{\rm exp}$ vs. the result predicted from the Lubchenko and Wolynes (LW) relation. The LW relation contains neither adjustable nor ambiguous quantities if the melting transition can be taken to be like that of the Lennard-Jones system. We see there is excellent agreement for the vast majority of the 44 substances for which we have all the relevant thermodynamic and kinetic data for the freezing and vitrification transitions. Only for eight substances is the error greater than 25%, while the dynamic range exhibited by

m and ΔC_p is a factor of 5 or so. With the eight outliers removed, the current correlation using T_m rather than T_g shows equally as tight a fit as that obtained by Wang and Angell with the same outliers missing; the R values of a best fit line are both 0.96.

Several aspects of Figure 2.1 are worthy of more careful attention. First we note that many of the extreme outliers are systems where the assumptions of the microscopic analysis are known to be violated in some way. Selenium, for example, is know to undergo a polymerization transition in the temperature range of the glass transition itselfsclearly a changing degree of polymerization would violate the fixed, near-spherical unit assumption. Decalin, TPP, and $H_2SO_4 \cdot 3H_2O$ undergo crystallization transitions to orientationally disordered, that is, they exist as plastic crystals or "glacial" liquid phases. In either case, the assumption of complete freezing of degrees of freedom in the crystal or release of degrees of freedom on melting would be violated. Even if we were to remove these outliers, it is clear that there are some modest but systematic deviations from the LW prediction. We must remember, however, that within the context of RFOT theory some such systematic deviation is to be expected.[45, 93] The XW estimate of the mismatch energy assumed a maximally sharp interface between the mobilized region and its environment. Two effects within RFOT theory should broaden this interface, and this would be expected to reduce the mismatch energy. One effect is that the proximity between T_A and T_g allows order parameter fluctuations to soften the barrier.[45] This is a temperature-dependent effect. Also, in more elaborate theories, the details of replica symmetry breaking ("wetting")[93] in the interface can change the surface cost and introduce another length scale. Only a modest change of the mismatch energy estimate would be needed to bring any of the measured substances into perfect agreement with theory. It appears, however, that overall a small hardening is needed. We should, however, also keep in mind that not all of the substances surveyed are so well modeled with Lennard-Jones attractions, and thus they may have different density changes on freezing which would modify their entropy of fusion. This is a likely contribution to the deviation from theory.

This survey of experimental data on simple molecular substances leads us to conclude that the empirical correlations of kinetic and thermodynamic data for glasses and supercooled liquids summarized in Angells notion of fragility are robust, at least for those

systems credibly modeled as interacting (fused) spheres. Others have raised concerns about the earlier empirical correlations for polymeric systems.[94] Yet the necessary information about crystallization for these polymer systems is hard to monitor, making the present method of analysis difficult.

While we have observed some molecule-specific deviations from the pattern of correlation between dynamics and thermodynamics, the observed correlation is extremely clear. Explaining these correlations, in our view and that of others, should be required of any microscopic theory of the glass transition in supercooled molecular liquids.[95] As we have shown here, the microscopic theory of glasses based on random first-order transitions not only predicts these robust trends but also provides quite accurate quantitative predictions of kinetic fragility from thermodynamics without the use of any adjustable fitting parameters for the 44 substances.

Chapter 2, in full, is a reprint of the material as it appears in the Journal of Physical Chemistry B 109 15093–15097 (2005), J. D. Stevenson and P. G. Wolynes. The dissertation author was the primary investigator and author of this paper.

Chapter 3

The shapes of cooperatively rearranging regions in glass-forming liquids

The cooperative rearrangement of groups of many molecules has long been thought to underlie the dramatic slowing of liquid dynamics upon cooling toward the glassy state. Laboratory evidence for cooperatively rearranging regions (CRR's) on the nanometer length scale has been obtained near the glass transition. The random first order transition (RFOT) theory of glasses predicts that, near T_g, these regions are compact, but computer simulations and experiments on colloids suggest CRR's are string like. We present a microscopic theory within the framework of RFOT that shows the shapes of cooperatively rearranging regions in glassy liquids should change from being compact at low temperatures to fractal or "stringy" as the dynamical crossover temperature from activated to collisional transport is approached from below. This theory predicts a correlation of the ratio of the dynamical crossover temperature to the laboratory glass transition temperature, and the heat capacity discontinuity at the glass transition, ΔC_p. The predicted correlation quantitatively agrees with experimental results for 21 materials.

The random first order transition (RFOT) theory of glasses, based on a secure sta-

tistical mechanical formulation at the mean field level[6, 10, 14, 26, 28, 96, 97, 15] explains the dynamics of supercooled liquids through the existence of compact, dynamically reconfiguring regions ("entropic droplets")[19, 21, 98] whose predicted size is very much consistent with what has been measured (125-200 molecules), using both optical methods[99], scanning microscopy[100, 101] and NMR techniques[102, 103], at temperatures near to T_g. Computer simulations[104, 105, 106, 107] and light microscopy studies of colloidal glasses[108] have revealed CRR's that are not compact, contain fewer particles, and are described as "fractal[109]" or as being "string" like[105, 106]. In this paper we will show that the fractal nature of the dynamically reconfiguring regions in the relatively high temperature regime probed in current computer simulations follows quite naturally from RFOT theory. While the CRR's are compact near the laboratory glass transitions, RFOT theory predicts strings will dominate near the higher dynamical crossover temperature, T_A, above which motions are no longer activated. This morphological transformation is shown in figure 3.1.

Computer simulations are carried out near the dynamical crossover. Likewise, colloidal glasses are inevitably studied near to the dynamic crossover because the large size of colloidal particles, in molecular terms, means that their nano-scale constituents intrinsically move more slowly than small molecules do.

According to our theory, the dynamical crossover from activated motion has a spinodal character[14, 110]. An analogous change of morphology predicted for nucleation clusters is thought to occur in ordinary first order transitions[111], so others have already suggested that the dynamical heterogeneities near T_A should be fractal[112]. The RFOT theory predicts the temperature range where the metamorphosis from compact to fractal happens for glassy liquids. RFOT theory predicts the gap between the dynamical crossover temperature and the glass transition temperature for molecular liquids should correlate inversely with the configurational heat capacity, as is found in experiment.

The mean field theory of RFOT theory starts by constructing aperiodic minima of a free energy functional[6] based on spatially varying density[7, 6, 113, 114]. These aperiodic free energy minima resemble the "inherent structures" that are minima of the potential energy[115]. At finite temperature, these aperiodic structures represent a compromise between the cost of localizing a particle TS_{loc} and the free energy gain realized by particles

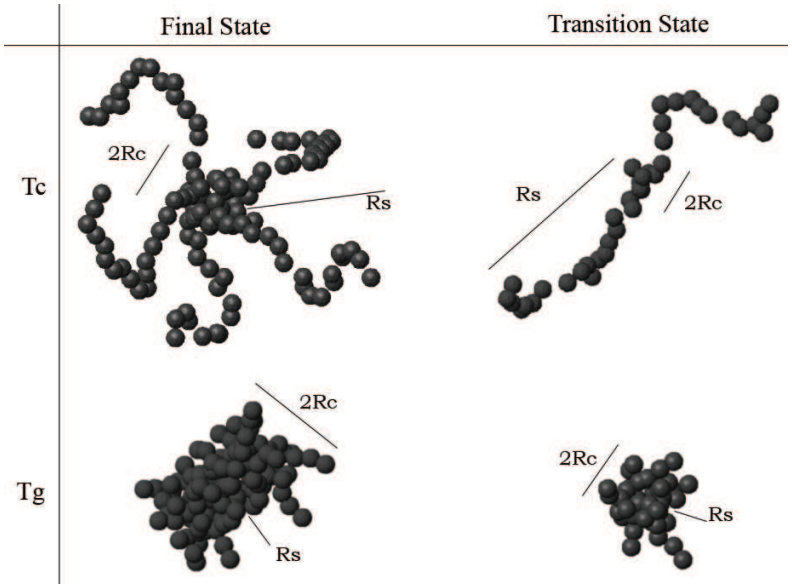

Figure 3.1: The shape of CRR's at T_g and T_c. The schematic appearance of the reconfiguring regions predicted by RFOT theory according to the free energy profiles of the fuzzy sphere model (see text) at the glass transition temperature, T_g, and the crossover transition temperature T_c^{string}. The shapes are shown for both the rearranged CRR (the final state) and the partially rearranged transition state.

being able to avoid each other once localized. The latter free energy contribution is represented by an interaction term in the usual free energy density functional. Any resulting localized, non-crystalline solution is only metastable. The difference of free energy of the typical localized solution and the uniform state is the configurational entropy times the absolute temperature[28].

To estimate the interactions, it was pointed out[21] that, at the Kauzmann temperature T_K where the configurational entropy vanishes, their total must equal the localization cost $T_K S_{loc}$. Therefore, if a typical molecule has z nearest neighbors a local interaction of pairs must contribute a term $v_{int} = (1/z)T_K S_{loc}$ on average. The localization entropy cost, in the free energy functional, depends logarithmically on the amount of space each molecule moves in while encaged: $S_{loc} = \frac{3}{2}k_B \log(\alpha_L/\pi e)$ where α_L is the inverse square of the Lindemann ratio of the r.m.s. vibrational amplitude in the glass to the intermolecular

spacing. The Lindemann ratio is predicted by detailed microscopic calculations[6, 7, 116] and agrees with neutron scattering measurements of the long-time plateau of the structure function. The ratio only weakly depends on the intermolecular potential and is of order $\frac{1}{10}$ near T_g. Thus v_{int} should be nearly the same in units of $k_B T_K$ for all molecular glass formers made of spherical particles. This near universality of the interaction per molecular unit allows RFOT theory to make quantitative predictions of glassy dynamics such as the typical barriers[21] near T_g, the degree of nonexponentiality[98] and the correlation length[21] near T_g.

The escape from a given aperiodic minimum resembles the dynamics of a random field Ising magnet (RFIM) in a biasing field. The free energy difference on a site predicted by the density functional plays the role of the magnetic field having a magnitude $TS_c(T)$. This quantity fluctuates, so the "field" fluctuations are of the order $\sqrt{k_B T \Delta C_p}$ where ΔC_p is the configurational heat capacity of the fluctuating region. The interaction between a pair of sites in the RFIM analogy is v_{int}, which is already computed. Using this quantitative mapping, RFOT theory can predict the typical escape barrier and it's fluctuations of the barriers near T_K.

The shape of a reconfiguring region is characterized by the number of contiguous sites N that are rearranged and the number of surface interactions that are broken, b. Near to T_K, the regions that dynamically reconfigure should be compact because this involves losing the smallest number of favorable interactions, b, will be lost while gaining the same configurational entropy proportional to N.

Maximal compactness implies a roughly spherical shape giving a free energy cost

$$\Delta F(N) = -TS_c N + v_{int}\frac{z}{2} 4\pi \left(\frac{N}{4\pi/3}\right)^{2/3} \tag{3.1}$$

This yields a barrier that diverges in three dimensions like S_c^{-2}. In analogy to the RFIM[20], near T_K the interface of the reconfigured region between any two aperiodic patterns will actually be wetted by other specific aperiodic minima that better match the two abutting regions than they do already. This effect lowers the surface energy term to scale like $N^{1/2}$ rather than $N^{2/3}$. This form for the mismatch energy restores the scaling relations near

T_K[19], and agrees with additional replica symmetry breaking in the interface found in replica instanton calculations[93, 97]. Wetting cannot occur at short ranges so the scale of this mismatch term still follows from v_{int}. In this way the observed Vogel-Fulcher scaling near T_K is predicted, $\Delta F^{\ddagger} \propto S_c^{-1}$ with the numerical proportionality coefficient depending on the microscopic value of $v_{int} = \frac{1}{z}\frac{3}{2}k_B T_K \log\frac{\alpha_L}{\pi e}$. The result is a universal multiple of $k_B T_K$. The resulting predicted absolute activation barriers agree well with experimental results for 44 substances[24, 45], a typical deviation being less than 20%.

The compact shape of the CRR and Vogel-Fulcher behavior are asymptotically correct only near T_K. Away from T_K the CRR need not be compact and deviations from the VF law occur. Non-spherical shapes have an entropy advantage; although the sphere (for which $b = \frac{z}{2}4\pi\left(\frac{N}{4\pi/3}\right)^{2/3}$) is unique, there are many contiguous structures with other shapes. Increased temperature favors these more ramified shapes as CRR's. Contiguous shapes, called lattice animals[117], have been enumerated and play a role in problems such as percolation[118] and Yang-Lee zeros[119]. Near a spinodal of an ordinary first order transition the dominant nuclei should be lattice animals characteristic of clusters at the percolation threshold[111].

Accounting for the multiplicity of possible shapes, the free energy of moving a CRR of N sites with b boundary interactions is

$$\Delta F(N,b) = -TS_c N + v_{int} b - k_B T \log(\Omega(N,b)) \tag{3.2}$$

where $\Omega(N,b)$ is the number of lattice animals of given N and b. For a given N the most numerous shapes are percolation-like. When these shapes dominate we can use enumerations near the percolation limit to evaluate $\Omega(N,b)$. In percolation clusters[118], for large N,

$$\Omega_{perc}(N,t) \sim \left(\frac{(\alpha+1)^{\alpha+1}}{\alpha^{\alpha}}\right)^{N} \exp\left(-\frac{N^{2\phi}}{2B^2}(\alpha-\alpha_e)^2\right) \tag{3.3}$$

Here, $\alpha = t/N$, and t is the number of unoccupied sites bounding the occupied cluster. We will take ϕ to have its mean field value of 1/2. B is a lattice dependent constant. $B = 1.124$ (for the face centered cubic lattice) follows from fitting to numerics calculated[120] for

clusters with $N \leq 9$. The mean value of t/N approaches $\alpha_e = (1 - p_c)/p_c$ for large N at the percolation threshold, p_c ($p_c = 0.198$[120] for the FCC lattice).

To evaluate the needed percolation quantities for random close packed lattices we must define a "contact." Spheres need not precisely touch (as in, say, percolation conductivity experiments), but rather their surfaces may be separated by at most a Lindemann length in order to be called connected. The parameters for this continuum percolation problem can be easily estimated since they primarily depend on the near neighbor connectivity. The number of neighbors in the rcp lattice is roughly the same as the face centered cubic (FCC); thus it is reasonable to use parameters for an FCC close packed lattice of spheres.

The number of bonds, b, is directly related to t. For the simple cubic lattice, $\frac{<b>}{<t>} = 1.67$[121] and the ratio should be linear in coordination number, z. Thus, for the rcp lattice with $z = 12$

$$\Delta F(N,t) = -TS_cN + v_{int}1.68\frac{z}{z_{SC}}t - k_BT\log(\Omega_{perc}(N,t)) \tag{3.4}$$

To find the dominant escape route and activation barrier we find the most probable t as a function of N. Minimizing equation 3.4 with respect to t, the most probable value of t is $\bar{t} = \bar{\alpha}N$ where $\bar{\alpha} = 3.10$. With this most probable value, Ω_{perc} becomes simply $\Omega_{perc} = \lambda^N$ where $\lambda = 7.64$. Each term in equation 3.4 is now proportional to N.

$$\Delta F(N) = k_BTN\left(-\frac{S_c}{k_B} + \frac{v_{int}}{k_BT}1.68\frac{z_{FCC}}{z_{SC}}\bar{\alpha} - \log(\lambda)\right) \tag{3.5}$$

Apart from S_c each term in this expression follows from a microscopic calculation. The free energy profile therefore only depends on the configurational entropy, and either monotonically increases or decreases with N. If the free energy profile increases with N, a reconfiguration event via a percolation cluster is impossible, so a more compact structure will eventually become stable for large N and provides the dominant reconfiguration route. If F decreases with N for the percolation shape, no barrier at all should be observed. The change of behavior of $\Delta F(N)$, from increasing to decreasing with N, signals a crossover to non-activated dynamics. Introducing the v_{int} determined by RFOT yields

$$\begin{aligned}\Delta F(N) &= k_B T N \left(-\frac{S_c}{k_B} + (3.20 - 1.91) \right) \\ &= -k_B T N \left(\frac{S_c}{k_B} - 1.28 \right)\end{aligned} \tag{3.6}$$

Accordingly barrier-less reconfigurations occur at a critical configurational entropy, $S_c^{perc} = 1.28 k_B$ if we neglect the mean field softening effects on v_{int}. Using the thermodynamic relation, $S_c(T) = \Delta C_p(T_g) T_g / T_K (1 - T_K/T)$, RFOT theory thus yields the crossover transition temperature, T_c^{perc}.

$$\frac{T_c^{perc}}{T_K} = \left(1 - \frac{S_c^{perc}}{\Delta C_p} \frac{T_K}{T_g} \right)^{-1} \tag{3.7}$$

The bigger ΔC_p is, the closer T_c^{perc} will be to T_K; more "fragile" liquids with larger ΔC_p have a smaller activated range, while a broader range for activated transport applies for stronger liquids with smaller ΔC_p. A similar trend is predicted for the mean field crossover based on detailed microscopic calculations for fluids with network network structure[116]. The entropy at the higher mean field crossover is $S_c(T_A) = 2.0 k_B$. Including the softening of v_{int} expected as this mean field transition is approached lowers the estimate of the percolation point. The amount of lowering is uncertain, however, because simultaneous with the softening a broadening of the interface is expected, thus effectively reducing the possible entropy gain from shape fluctuations. We see that the transition occurs at the same configurational entropy level whether the liquid be fragile or strong. As in the RFOT theory of the non-exponentiality parameter β[98], fluctuations in the driving force depend on ΔC_p explicitly and should be included in equation 3.1. Thus fast and slow CRR's would have somewhat different shapes (faster being more ramified generally since their entropy is higher).

Counting percolation clusters is not all that different from finding the statistics for strings. The crossover transition argument can be carried out for purely string-like objects as follows. The number of broken interactions of a string scales with length, $N(z-2)$, as does the shape entropy of a string, $\log(\Omega) = N \log(z-5)$. $(z-5)$ represents the number of directions a string can take that excludes backtracking on top of, or directly next to,

the previous particle leading to a compact cluster. Using these coefficients we find that string growth becomes down hill at an entropy of $S_c^{string} = 1.13k_B$. The predicted crossover temperature is

$$\frac{T_c^{string}}{T_K} = \left(1 - \frac{S_c^{string}}{\Delta C_p}\frac{T_K}{T_g}\right)^{-1} \tag{3.8}$$

a bit lower than predicted by percolation. In Figure 3.2a we plot the predicted T_c^{string} and T_c^{perc} versus $1/\Delta C_p$ for various liquids. Crossover temperatures from activated to non-activated dynamics were determined by using Stickel plot analysis[122]. The experimental crossover temperatures for 21 substances obtained in this way by Novikov and Sokolov[123] are plotted in the figure along with the RFOT prediction. Some of the outliers are polymers for which other slowing effects compound simple RFOT results. Uncertainty in T_K for very strong liquids probably is a source of the discrepancy between the theory and experiment for these latter substances. We also plot $(T_c - T_g)/T_g$ in figure 3.2b. According to RFOT theory the entropy at T_g is $S_c(T_g) = \Delta C_p(T_g - T_K)/T_K = 0.79k_B$. Corresponding to a glass transition at $10^{10}P$ (see figure 3.4). The quantitative agreement of the experimental crossover temperatures and the present predictions of the string and percolation transitions is striking.

To quantify the typical shapes of reconfiguring regions at temperatures between T_c and T_K we must have a suitable analytic form of $\Omega(N, b)$ for all relevant values of N and b. Surface roughening theories give predictions of $\Omega(N, b)$ valid for nearly spherical objects[124], but would be useful only near T_K. On the other hand, the percolation theory gives an explicit form of Ω valid only for the most populous ramified, fractal shapes that dominate near the crossover.

A reasonably effective, but unabashedly approximate, treatment of the animal counting problem interpolates smoothly between these limits. We take the reconfiguring region to be a "fuzzy sphere," a spherical core of n_c particles, surrounded by a ramified, but connected, halo of n_f particles. If we let the core size, n_c, vanish we are left with only an extended object. Conversely, if the halo size vanishes then we have only a sphere. The halo resembles a percolation cluster, but we will describe it as a set of strings of

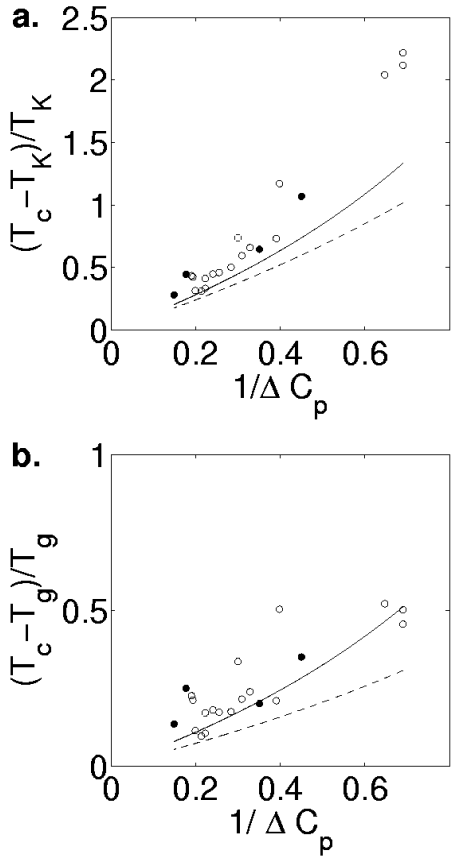

Figure 3.2: Predictions for the crossover temperatures. **a**. Predictions for $(T_c^{string} - T_K)/T_K$ (dashed line) and $(T_c^{perc} - T_K)/T_K$ (solid line). The experimentally derived crossover temperatures, $(T_c^{exp} - T_K)/T_K$, from Novikov and Sokolov[123], are shown as circles with the dark circles referring to polymers. In all cases the values for the Kauzmann temperature, T_K, were taken from the correlation[125] $T_K = T_g(1 - 16/m)$. **b**. Same as for **a**. except a plot of $(T_c - T_g)/T_g$.. The conversion ratio T_K/T_g was set through $S_c(T_g) = \Delta C_p(T_g - T_K)/T_K = 0.79k_B$. For both plots the ΔC_p values for the materials were determined from their m values through the correlation $m = 20.7\Delta C_p$ discussed in Stevenson and Wolynes[24].

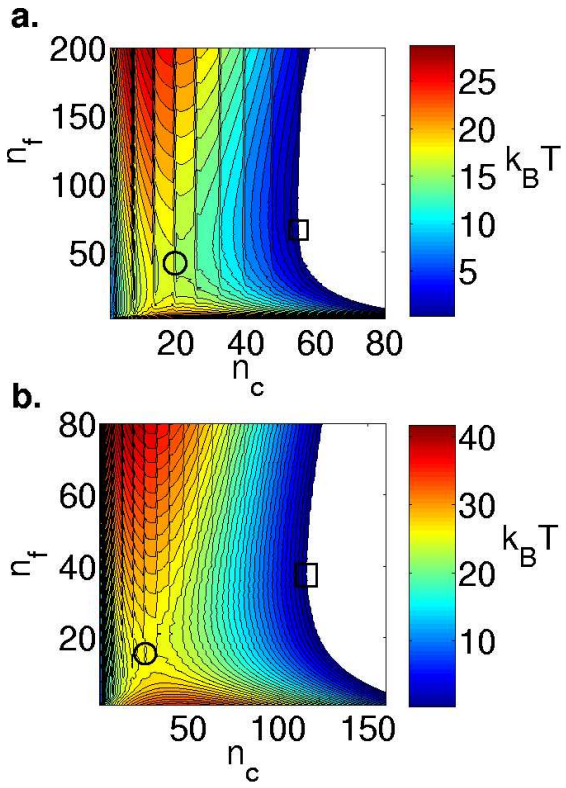

Figure 3.3: Free energy contours for the fuzzy sphere model. Two dimensional free energy profiles as functions of the number of particles in the core, n_c, and the number in the fuzzy halo, n_f, **a**. near T_c^{string} and **b**. near T_g. The sidebar is in units of k_BT with the contours lines corresponding to intervals of $1k_BT$. The circles indicate the location of the typical transition state. The squares indicate a fully reconfigured region.

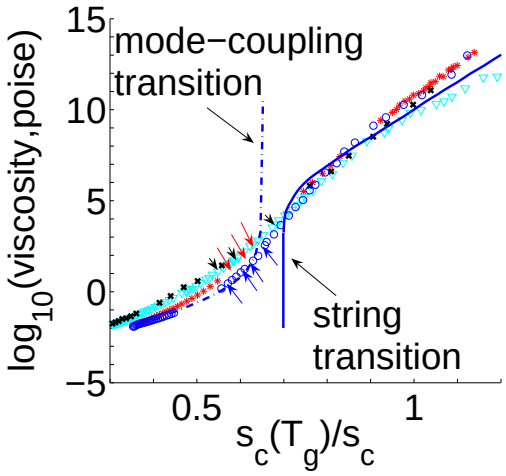

Figure 3.4: Predicted and experimental viscosity. A comparison of experimental viscosity with the barriers predicted from the fuzzy sphere model (solid line). Data for Salol[122], Propylene Carbonate[122] O-Terphenyl[126, 127], and alpha-Phenyl-O-Cresol[126, 127] are represented as circles, crosses, stars and triangles respectively. An experimental mode coupling fit to salol[128] is shown with a dot-dashed line. Experimentally derived values of the entropy at the crossover transitions[123] are shown with arrows. The free energy barriers were placed on the $log_{10}(viscosity)$ curve by setting $\Delta F^{\ddagger} = 0$ to correspond with the large T experimental value of 1 centipoise for the viscosity. A viscosity of $10^{10}P$ was used to determine the theoretical value $S_c(T_g) = 0.79k_B$.

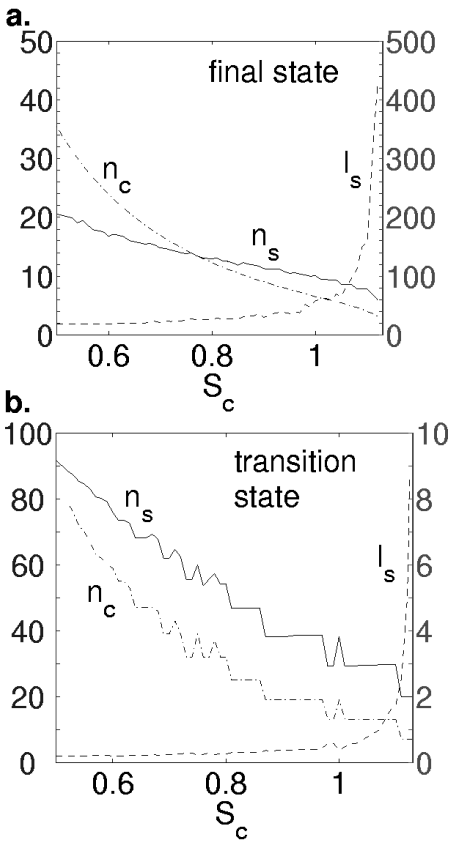

Figure 3.5: Shape Characteristics for the fuzzy sphere. The characteristics are shown as functions of the configurational entropy for the final state and the transition state. n_c (dashed-dotted line) is the number of particles in the core, n_s (solid line) is the number of strings and l_s (dashed line) is the typical length of a string. **a**. The final state: n_c uses the axes on the right while n_s and l_s use the axes on the left. **b**. The transition state: here n_s uses the axes on the right while n_c and l_s (dashed line) use the axes on the left. The sizes and lengths are given in terms of the number of particles.

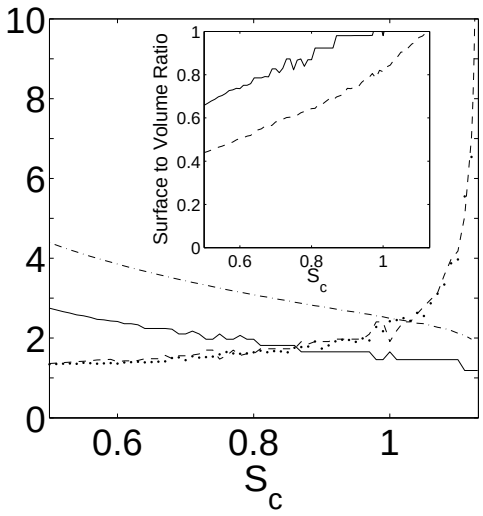

Figure 3.6: Radial dimensions of the fuzzy sphere. The radius of the core, R_c, at the transition state (solid line) and at the final state (dashed-dotted line). Also, the radius of the stringy halo, R_s, at the transition state (dashed line) and the final state (dotted line). The radii are given in terms of the number of particles. The inset gives the surface to volume ratio of the fuzzy sphere normalized to that of an infinite string. The solid line is the final state while the dashed line is the transition state. Both plots are shown vs. the configurational entropy, S_c.

particles extending from the surface of the central core, since we can determine the entropic contribution of a halo of n_s strings.

Using the resulting fuzzy sphere entropy we can find the full activation free energy profile.

$$\begin{aligned}\Delta F(n_c, n_f, n_s) =& v_{int}\frac{z}{2}\left(\frac{4\pi/3}{n_c}\right)^{1/6}\left(4\pi\left(\frac{n_c}{4\pi/3}\right)^{2/3} - n_s\right) + v_{int}(z-2)n_f \\ &- TS_c(n_c + n_f) - k_B T log(\Omega(n_c, n_f, n_s))\end{aligned} \tag{3.9}$$

$$\Delta F(n_c, n_f) = -log\left(\sum_{n_s} exp(-\Delta F(n_c, n_f, n_s))\right) \tag{3.10}$$

In the supplementary material you can find the full expression for the fuzzy sphere entropy, Ω, accounting for the excluded volume between the strings[129]. Figures 3.3a and 3.3b show contour plots of the free energy at a configurational entropy value near the dynamic crossover and near the glass transition respectively. The saddle points on these free energy surfaces describe transition state ensembles for reconfiguration. The predicted barrier still depends universally on the configurational entropy as shown in figure 3.4. We also show the experimental barriers for liquids of varying fragility. The universal dependence on configurational entropy is clearly confirmed (In these plots the calorimetrically determined T_g's were used for calibration, not the viscometric values!). At low T the barrier clearly depends linearly on $1/S_c$ for $S_c < S_c^{string}$ consistent with the asymptotic RFOT analysis, but as the critical value of the configurational entropy, S_c^{string}, is approached the activation barrier rapidly decreases, dropping to zero at S_c^{string}. The experimental mode coupling fit to the viscosity[128] shows a striking symmetry. The mode coupling theory fits the dynamic transition from above, while the current argument predicts its emergence from below.

The shapes of CRR's are broadly distributed as shown via the broad $1k_BT$ contour in the plots. Examples of the final shape expected near T_g and near the crossover temperature are shown in figure 3.1. To quantify specifically the characteristic final shape, we take it to be the one with the smallest core. Figures 3.5 and 3.6 show how the resulting scales of the transition states and CRR's change with configurational entropy. Near T_g the shapes

are mostly spherical with just a small fraction of the particles in the stringy halo. This size agrees with the previous XW estimate. They consist of around 125 particles (beads) near T_g, and are thus bigger than the CRR's invoked in the venerable Adam-Gibbs approach[5]. This prediction of RFOT theory received dramatic confirmation in an experimental study by Berthier. et al[23]. They show that multi-point correlations near T_g correspond to a correlation length of about 5 units, independent of fragility. A typical protuberance on the compact core near T_g contains only 2 particles. Near T_c^{string}, however, the core size becomes very small while the strings lengthen dramatically. This growth occurs for both the transition state and the final state. A powerful probe that should be able determine the shape of the cooperatively rearranging regions is a version of the spin diffusion NMR experiment of Tracht et. al.[130] The spin diffusion between neighboring slow and fast regions directly measures the surface to volume ratio which changes as the CRR's change from compact to stringy. We show our prediction of this ratio in the inset of figure 3.6.

The string lengths near T_c^{string} are larger than those usually reported in simulations or in microscopy. This apparent discrepancy arises from a kinetic effect as follows: Though the free energy barrier for creating a string approaches zero at T_c^{string}, the actual time to construct a string grows with the length of the string. The barrier to create a new string is somewhat larger than to extend an old one. Because of this, the growth/death of a string takes place particle by particle on the microscopic time scale, and should be diffusive, with growth time $\tau_s = \tau^0_{micro} l_s^2$. Here, τ^0_{micro} is a typical vibrational time scale, i.e.the time for a particle to explore its cage. When τ_s becomes comparable to the time for another activated event to occur in the immediate vicinity of the string, τ_α / l_s, the growth of the original string will be interrupted. Here, $\tau_\alpha = \tau^0_{micro} e^{F^\ddagger / k_B T}$. This finite growth time gives a maximum limit for the length of strings:

$$l^3_{s,max} = e^{F^\ddagger / k_B T}. \tag{3.11}$$

Larger strings will be interrupted, or "incoherent," since an activated event occurs along the string. This phenomenon of "incoherent" strings is seen in simulations[105]. Using the fuzzy sphere model, the minimum barrier corresponds to a core region with 7 particles. This gives an $F^\ddagger$ consistent with what Novikov and Sokolov[123] call the "magic" relaxation time

for the crossover and a length $l_{s.max} \cong e^{14/3} \cong 108$. While larger than the lengths usually quoted from simulations, the rapid variation of $F^{\ddagger}$ and l_s near the string transition makes this result rather sensitive to modeling details. The key is that there is a natural cut off of kinetic origin that causes T_c^{string} to be a crossover and not a sharp transition.

We see that the random first order transition theory predicts CRR's are compact, nearly spherical objects in the deep supercooled region, but that in the moderately supercooled region, near the mode coupling transition, the CRR's become non-compact, extended string-like objects. The crossover temperature is entropically controlled allowing the prediction of the dynamic crossover temperature. This result is confirmed by experiment.

Chapter 3, in full, is a reprint of the material as it appears in Nature Physics 2 268–274 (2006), J. D. Stevenson, J. Schmalian, and P. G. Wolynes. The dissertation author was the primary investigator and author of this paper.

Chapter 4

Theory of secondary relaxations in supercooled liquids and structural glasses

Diversity, a key feature of glassy systems, is most apparent in their relaxation properties. Dielectric, mechanical and calorimetric responses of supercooled liquids to perturbations are not single, simple exponentials in time, but manifest a distribution of relaxation times. The typical relaxation time grows upon cooling the liquid until it exceeds the preparation time, yielding a non-equilibrium glass, which can still relax but in an age dependent fashion. In addition to the main relaxations that are responsible for the glass transition, supercooled liquids and structural glasses exhibit faster motions, some of which are distinct enough in time scale from the typical relaxation to be called "secondary" relaxation processes[131, 132, 133, 134, 135]. These faster motions account for only a fraction of the relaxation amplitude in the liquid but can become the dominant features in the relaxation of otherwise frozen glass, being then of central importance to the glass's mechanical properties. These secondary relaxation processes in the solvation shell of proteins are also prominent in the study of protein dynamics[136].

The phenomenology of secondary relaxation in glassy systems has been much dis-

cussed but it is perhaps not a surprise that, owing especially to the problem of how to subtract the main peak, the patterns observed seem to be more complex and system specific than those found for the main glassy relaxation. Nevertheless while some of the secondary relaxation motions are, doubtless, chemically specific, occurring on the shortest length scales, the presence of secondary relaxation in glassy systems seems to be nearly universal[137]. In this paper we will show how secondary relaxations naturally arise in the random first order transition (RFOT) theory of glasses[138] and that these universally expected relaxations are predicted to scale in intensity and frequency in a manner consistent with experimental observations.

The random first order transition theory of glasses is based on the notion that there is a diversity of locally frozen free energy minima that can inter-convert via activated transitions. The inter-conversions are ultimately driven by an extensive configurational entropy. RFOT theory, which can be formulated at the microscopic level, accounts for the well known correlations between the primary relaxation time scale in supercooled liquids and thermodynamics[21, 24] as well as the aging behavior in the glassy state[22]. By taking account of local fluctuations in the driving force, RFOT theory also gives a good account of the breadth of the rate distribution of the main relaxation[98, 139]. In this paper we will argue that, universally, a secondary relaxation also will appear in the relaxation of glass forming liquids and that its intensity and shape depends on the configurational thermodynamics of the liquid. This relaxation corresponds with the low free energy tail of the activation barrier distribution. The distinct character of this tail from the main relaxation, however, comes about because the geometry of the reconfiguring regions for low barrier transitions is different from that of those rearranging regions responsible for the main relaxation. In RFOT theory, near to the laboratory T_g, the primary relaxation process involves reconfiguring a rather compact cluster. The reconfiguring clusters become more ramified as the temperature is raised and eventually begin to resemble percolation clusters or strings near the dynamical crossover to mode coupling behavior, which can be identified with the onset of non-activated motions[140]. Reconfiguration events of the more extended type are considerably more susceptible to fluctuations in the local driving force, even away from the crossover. Owing to this, as we will show these ramified or "stringy" reconfiguration events

generally dominate the low barrier tail of the activation energy distribution.

In this paper we will examine the effect of driving force fluctuations on reconfiguration barriers when the shape distribution of reconfiguration processes is accounted for. A simple statistical computation shows that a two peaked distribution of barriers can arise from this shape distribution. This calculation motivates a more explicit but approximate theory that gives analytical expressions for the distribution of relaxation times in the tail. In keeping with experiment, the theory predicts the secondary relaxation motions are actually most numerous near the crossover, but of course, merge in frequency with the main relaxation peak in time scale also at that crossover. Furthermore the relaxation time distribution for secondary relaxations is predicted to be described by an asymptotic power law. The theory is easily extended to the aging regime where these secondary relaxations can dominate the rearranging motions.

In random first order transition theory, above the glass transition temperature, the entropic advantage of exploring phase space manifests itself as a driving force for reconfiguration balanced by a mismatch energy at the interface between adjacent metastable states. For a flat interface in the deeply supercooled regime the mismatch energy can be described as a surface tension that can be estimated from the entropy cost of localizing a bead[19, 21]. This estimate gives for the surface tension $\sigma_0 = (3/4)k_BTr_0^{-2}\ln[1/(d_L^2\pi e)]$ where d_L is the Lindemann length, the magnitude of particle fluctuations necessary to break up a solid structure, and is nearly universally a tenth of the inter-particle spacing, ($d_L = 0.1r_0$). The mismatch energy cost is therefore about the same for all substances. The free energy profile for reconfiguration events can be described by equations that resemble nucleation theory at first order transitions but are conceptually quite distinct. Following Stevenson-Schmalian-Wolynes[140] the free energy cost of an N particle cluster with surface area Σ making a structural transition to a new metastable state may be written

$$F(N,\Sigma) = \Sigma\sigma_0 - Nk_BTs_c - k_BT\ln\Omega(N,\Sigma) - \sum_{\text{particles}}\delta\tilde{f} \tag{4.1}$$

For an arbitrarily shaped reconfigured region there is no simple relationship between Σ and N. A key element of the reconfiguration free energy profile is the shape entropy

$k_B \log \Omega(N, \Sigma)$ which accounts for the number of distinct ways to construct a cluster of N particles having surface area Σ. At one extreme are compact, nearly spherical objects with shape entropy close to zero. At the other extreme are objects such as percolation clusters or stringy chains whose surface area and shape entropy grow linearly with size N. The last term of equation 4.1 accounts for the inherent spatial fluctuations in the disordered glassy system manifesting themselves as fluctuations in the driving force. Local fluctuations in the surface mismatch free energy are ignored in this calculation[18, 17, 139], but their inclusion would not qualitatively alter the results. We simplify by assuming uncorrelated disorder, i.e. for each particle joining the reconfiguration event a random energy, $\delta\tilde{f}$, drawn from a distribution of width δf is added to the free energy profile. The root mean square magnitude of the driving force fluctuations above T_g is derived from the configurational entropy fluctuations which follow from the configurational heat capacity through the relation $\delta f \approx T\sqrt{\Delta C_p k_B}$, a result expected for large enough regions. We will assume no correlations for simplicity, but they can be included.

For reconfiguring regions forming compact, nearly spherical clusters the shape entropy is very small and the mismatch free energy is $\sigma_0 4\pi(3N/(4\pi\rho_0))^{\theta/3}$ with $\theta = 2$ if fluctuations are small. In disordered systems the mismatch free energies grow with exponent θ generally less than 2 reflecting preferred growth in regions of favorable energetics and the large number of metastable states which can wet the interface and reduce the effective surface tension. A renormalization group treatment of the wetting effect[19] suggests that $\theta = 3/2$ in the vicinity of an ideal glass transition. Incomplete wetting giving strictly $\theta = 2$ asymptotically would not change the numerics of the present theory much. Whether complete wetting occurs for supercooled liquids under laboratory conditions is still open to debate[16, 141, 17]. The free energy profile describing reconfiguration events restricted to compact clusters becomes, then, $F_{\text{compact}}(N) = \sigma_0 4\pi(3N/(4\pi\rho_0))^{\theta/3} - NTs_c$. The minimum number of particles participating in a stable reconfiguration event is determined by finding where the free energy profile crosses zero. The activation free energy barrier results from the maximum of the free energy profile and is inversely proportional to the configurational entropy, leading to the form suggested by Adam and Gibbs[5] for the most probable relaxation time $F^{\ddagger}/k_B T \sim \ln \tau_\alpha/\tau_0 \sim s_c^{-1}$. Adding driving force fluctuations to the profile

of compact reconfiguration events yields an approximate Gaussian distribution of barriers with width scaling as $\sqrt{N^{\ddagger}}\delta f$. Xia and Wolynes[98] have shown that, with the inclusion of facilitation effects, the resulting distribution of barriers accounts for the stretching of the main relaxation process and yields good estimates for how the stretching exponent varies with liquid fragility[142].

In the other extreme of shape, restricting the reconfiguration events to stringy clusters (using percolation clusters gives very similar results), the free energy profile is linear in the number of particles reconfigured, save for the minimum cost F_{in} to begin to reconfigure a region:

$$F_{\text{string}}(N) = -NT(s_c - s_c^{\text{string}}) + F_{\text{in}}. \tag{4.2}$$

The critical "entropy" is given by $Ts_c^{\text{string}} = v_{int}(z-2) - k_BT\ln(z-5) \approx 1.13k_BT$. This is the difference between the surface energy written in terms of the coordination number of the random close packed lattice $z \approx 12$ (v_{int} is the surface tension per nearest neighbor) and the shape entropy including Flory excluded volume effects[129]. If a single bead can reconfigure then the cost to begin to reconfigure a region is $F_{\text{in}} = zv_{int} - Ts_c \approx 2.5 - 2.9k_BT$. If two must be moved then $F_{\text{in}} \approx 6.1k_BT$. Some uncertainty in this estimate is noted in that the continuous form of the surface mismatch energy gives a somewhat higher value when applied to these small regions, giving $F_{\text{in}}^{\text{continuous}} = r_0^2\sigma_0 4\pi(3/(4\pi))^{\theta/3} - Ts_c \approx 10.5k_BT$ for a one particle reconfiguration. The remarkably simple free energy profile of equation 4.2 indicates that below T_{string} (defined by $s_c(T_{\text{string}}) = s_c^{\text{string}}$) the free energy monotonically increases and so reconfiguration via pure stringy objects is impossible, while above T_{string} the same process can occur with very small free energy barrier, having only to overcome F_{in}. Thus T_{string} signals the crossover from dynamics dominated by activated events to dynamics dominated by non-activated processes. Interestingly, this crossover is mathematically analogous to the Hagedorn transition of particle theory[143]. The predicted constant value of s_c^{string} agrees well with the crossover for the 21 materials for which data are available[140]. In contrast to the situation for compact reconfiguration, including driving force fluctuations dramatically affects the picture of stringy relaxation. Without fluctuations, stringy reconfiguration is impossible below the string transition T_{string}. With driving force fluctuations a

lucky sequence of fluctuations can easily push the nominally linearly increasing free energy profile to cross zero, the situation needed for a stable reconfiguration.

Stevenson-Schmalian-Wolynes[140] introduced a crude model to estimate the shape entropy and surface area of the wide range of shapes between the two extremes. This "fuzzy sphere" model, consists of a compact center of N_c particles with a stringy halo of N_f particles. With this interpolative model it was shown that near T_g the preferred shape of a reconfiguring region is largely compact, while the relevant regions become more ramified close to the dynamic crossover temperature. Fluctuations, aggregated cumulatively in the compact core yielding a variance proportional to N_c, and cumulatively in the stringy halo yielding a variance proportional to N_f, modify the local two dimensional free energy landscape. The local free energy plots for several realizations of these accumulated fluctuations, assumed to have Gaussian statistics, are given in figure 4.1. They show the paths available for the liquid to undergo a stable reconfiguration event. For some realizations compact reconfiguration will be required to overcome the free energy barrier. For other realizations the fluctuations are such that the free energy cost for reconfiguration crosses zero along the N_f axis (shown in the figure in yellow) signifying that the region is able to relax via a string-like reconfiguration event. These stringy rearranging clusters, stabilized by disorder, we argue are main contributors to the secondary relaxation process. The statistics of the stable reconfiguration paths with lowest free energy barrier gives rise to distributions of activation barriers as illustrated in figure 4.2 for two different values of δf corresponding to a strong and a fragile liquid. We can dissagregate these distributions into the parts due, separately, to the compact events ("primary") and to the string-like fluctuation induced events ("secondary"). These distributions are shown in figures 4.3 and 4.4 for a strong and fragile liquid respectively. At low temperatures primary relaxation is the dominant mode of reconfiguration, but as the temperature increases, fluctuations are able to stabilize string-like reconfiguration more easily and the secondary relaxation peak increases in prominence, apparently dominating at and above the string transition. At the same time, with increasing temperature, the primary relaxation peak shifts to lower free energy barriers making it difficult to distinguish between the two peaks in the overall distribution. As the dynamical crossover temperature is approached and crossed, the primary and secondary peaks

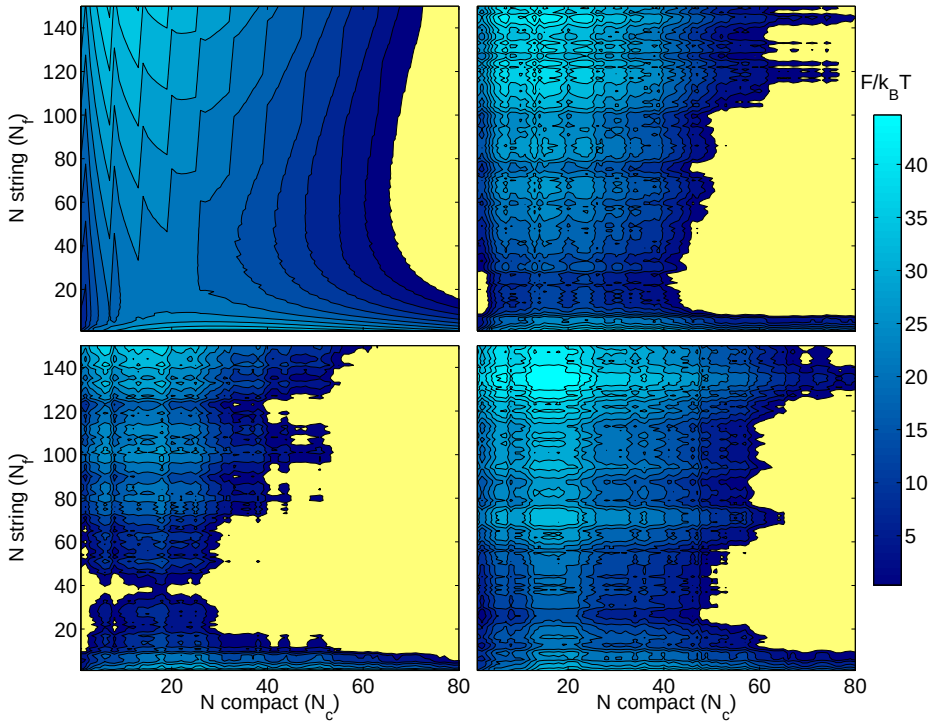

Figure 4.1: The two dimensional free energy profile describing cooperative relaxation as a function of the number of compact particles N_c and the number of stringy particles N_f in the reconfiguring region. The transition state separating the unreconfigured state ($N_c = N_f = 0$) with the final stable state (colored yellow in the figure) determines the free energy barrier to reconfiguration. The upper left panel gives the profile ($s_c = 1.0k_B$) in the absence of fluctuations while the others demonstrate three possible realizations of fluctuations for a relatively strong liquid, a liquid having $\Delta C_P \approx 1k_B$ per bead. The fluctuations for the two dimensional profile are implemented as cumulative sums of local fluctuations in both N_c and N_f. For the situation described in the bottom right panel compact reconfiguration is required to overcome the free energy barrier. For the two other realizations the fluctuations are such that stable (yellow) regions exist along the vertical axis, meaning string-like reconfiguration is possible. These stringy clusters, stabilized by fluctuations, account for the secondary relaxation.

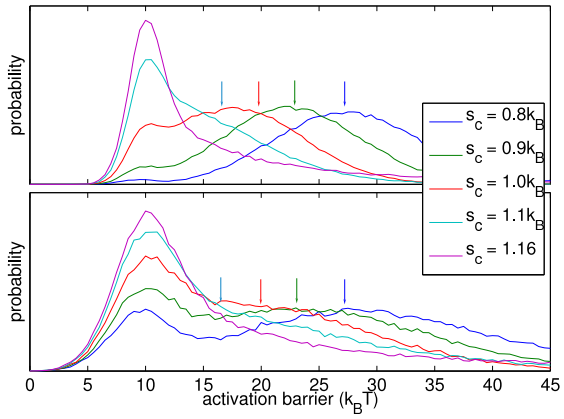

Figure 4.2: Probability distribution of free energy barriers governing relaxation events in supercooled liquids. Different curves represent different temperatures, increasing from near the glass transition temperature to near the dynamical crossover temperature. The arrows indicate the typical relaxation time predicted from the fuzzy sphere model without fluctuations. The dashed line gives the distribution of free energy barriers for a liquid just above the dynamical crossover temperature where primary relaxations disappear leaving only the secondary process. The top panel corresponds to a rather strong liquid with small fluctuations, $\Delta C_P \approx 1k_B$ per bead — a material similar to GeO_2. The bottom panel corresponds to a fragile liquid with larger fluctuations, $\Delta C_P = 3k_B$ per bead — a material similar to ortho-terphenyl. Secondary relaxations, i.e. relaxation events using string-like rearranging regions, increase in prominence as the temperature is increased, becoming the dominant process near the dynamical crossover temperature where the two peaks merge. The units of the activation energy are given in k_BT, which assumes a mismatch penalty primarily entropic in nature, $\sigma_0 \sim k_BT$. An energetic mismatch penalty, $\sigma_0 \sim k_BT_K$, would lead to Arrhenius behavior for the secondary relaxation process, as the distribution is peaked around the minimum free energy to initiate a stringy reconfiguration, $F_{\rm in}$. In this calculation we have used the continuous approximation of $F_{\rm in}$ shown in the text. The facilitation phenomenon, as described by Xia and Wolynes[98] and by Bhattacharya et al.[142] but not accounted for here, would shift weight from the largest free energies to the center of the primary peak, raising the overall height of the primary peak relative to the secondary peak.

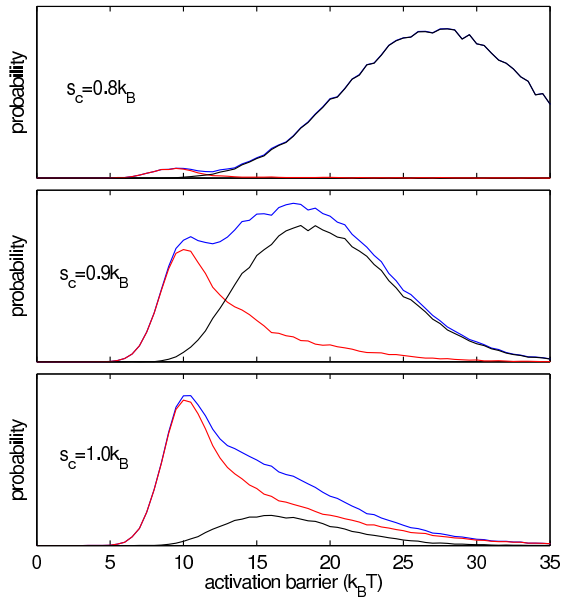

Figure 4.3: Distribution of free energy barriers for a strong liquid ($\Delta C_P \approx 1k_B$ per bead) separated into the contribution from secondary relaxations (red curves), corresponding to string-like reconfiguration as in panels b and c of figure 4.1, and primary relaxations (black curves), corresponding to compact reconfigurations. The full distributions are given for comparison (blue curves). The separation of the curves makes clear that as the dynamical crossover temperature is approached the primary relaxation becomes subordinate to the secondary relaxation.

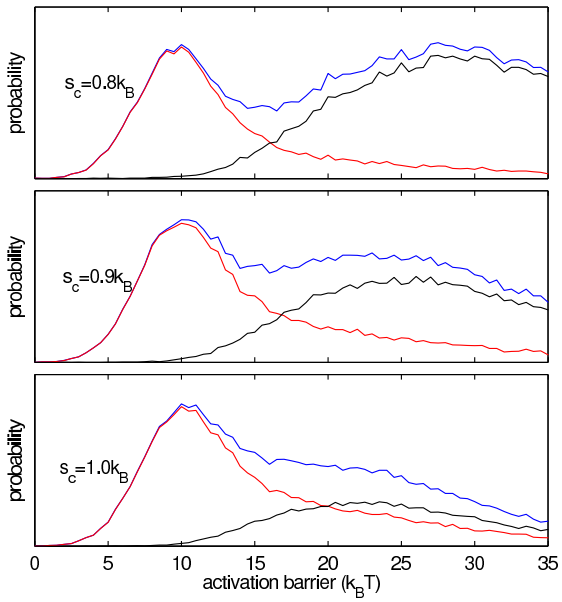

Figure 4.4: The corresponding results to those of figure 4.3 but for a fragile liquid, one with $\Delta C_P \approx 3k_B$ per bead.

merge with string-like reconfiguration clusters becoming the dominant mode of relaxation. For fragile liquids, i.e. liquids with larger configurational entropy fluctuations[24], the secondary relaxation peak is generally more important than for strong liquids. Both peaks are broader and begin to merge at lower temperatures for the more fragile liquids. Because facilitation effects are not explicitly accounted for (these would mostly affect the higher barriers) it is not easy to directly compare these distributions with quantitative precision to experiment. In addition, the number of reconfiguring particles in the two peaks is different, so their contribution to the measured dissipation is different as well. Nevertheless, the relative magnitude of the secondary relaxation peak predicted by this calculation as compared to the primary peak seems to be somewhat larger than experiments apparently show. This disparity is more pronounced for fragile materials that have larger fluctuations. The assumptions in the fuzzy sphere model, and especially the assumption of uncorrelated disorder, apparently overestimate the influence of the fluctuations, which are probably (anti-) correlated for the most fragile systems.

The distribution of free energy barriers for reconfiguration events that take an

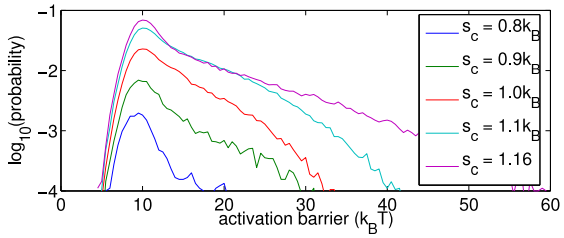

Figure 4.5: Distribution of free energy barriers for the secondary relaxation process from the statistical sampling of the fuzzy sphere model with fluctuations. The data correspond to a strong liquid ($\Delta C_P \approx 1$) and show that at higher temperatures (larger configurational entropies) the distribution decays more slowly. This leads to wider activation energy distributions, matching the expectations of the analytical calculations.

ideal stringy form can be explicitly calculated. A similar analysis to the string case can be applied to reconfiguration via percolation clusters but with somewhat different numerical constants in the relation of the free energy profile to N. This analytic calculation resembles that of Plotkin and Wolynes for the "buffing" of protein folding energy landscapes[144]. The key to the calculation of $\Gamma(F^{\ddagger})$, the distribution of free energy barriers governing reconfiguration events with less than $N_{\max}$ displaced atoms, lies in mapping the problem onto a random walk, or a diffusion process in free energy space. Going to the limit of continuous number of particles we may write a stochastic differential equation for the free energy profile $dF/dN = dF_{\text{string}}/dN + \delta\tilde{f}$. The principal quantity to compute is the Greens function, $G(N, F^{\ddagger}; F_{\text{in}})$ the probability that a reconfiguration path of N particles has free energy F if the cost to initiate the reconfiguration event is F_{in}. The evolution of G, that follows from the stochastic profile, may be described by a diffusion equation with drift subject to absorbing boundary conditions at both $F = 0$ and $F = F^{\ddagger}$. These boundary conditions permit the calculation of the distribution of free energy barriers by keeping track of the maximum excursion of the random walk.

$$\frac{\partial G}{\partial N} + \phi\frac{\partial G}{\partial F} = \frac{1}{2}\delta f^2\frac{\partial^2 G}{\partial F^2}, \tag{4.3}$$

The slope of the mean free energy profile $\phi = T(s_c^{\text{string}} - s_c)$ depends simply on the proximity to the string transition. ϕ is a string tension reflecting the free energy cost of lengthening a

string. The probability density for the maximum excursion of F, i.e. the free energy barrier is then

$$\Gamma(F^{\ddagger}) = -\frac{\partial}{\partial F^{\ddagger}} \int_0^{N_{max}} dN \left\langle \frac{\delta f^2}{2} \left. \frac{\partial G}{\partial F} \right|_{F=0} \right\rangle_{0<F_{\rm in}<F^{\ddagger}}. \tag{4.4}$$

In the above equation the average $\langle\cdot\rangle_{0<F_{\rm in}<F^{\ddagger}}$ is present to integrate over the fluctuations in the free energy cost of initiating a string — essentially capturing the statistics of the smallest possible activation barriers. The derivative with respect to $F^{\ddagger}$ converts from the cumulative probability that the free energy barrier is below $F^{\ddagger}$ to the probability the free energy barrier is between $F^{\ddagger}$ and $F^{\ddagger} + dF^{\ddagger}$. The Green's function can be calculated explicitly by solving the diffusion equation using the method of images. The result may be represented in closed form in terms of the Jacobi theta function, however we leave the sum explicit to more easily examine the asymptotics

$$\begin{aligned} G =& \frac{e^{\frac{\phi}{\delta f^2}(F - F_{\rm in} - \phi N/2)}}{\sqrt{2\pi \delta f^2 N}} \\ & \times \sum_{n=-\infty}^{\infty} \left[e^{-\frac{(2nF^{\ddagger} + F - F_{\rm in})^2}{2\delta f^2 N}} - e^{-\frac{(2nF^{\ddagger} + F + F_{\rm in})^2}{2\delta f^2 N}} \right] \end{aligned} \tag{4.5}$$

In the integral of equation 4.4 the cutoff $N_{\rm max}$ reflects the maximum size to which a stringy reconfiguration event would typically grow before compact rearrangements dominate. We estimate this maximum length as $N_{\rm max} \approx F_{\alpha}^{\ddagger}/\phi$, since certainly by that length the most important reconfiguration events would be compact and would contribute to the primary relaxation peak. A useful and accurate simplification of equation 4.4 can be made by smoothing the cutoff so that the finite integral $\int_0^{N_{\rm max}} dN \cdot$ is replaced by $\int_0^{\infty} dN \exp(-N/N_{\rm max}) \cdot$. The smoothed probability distribution of free energy barriers follows directly from equations 4.4 and 4.5

$$\Gamma = \frac{\partial}{\partial F^{\ddagger}} \left\langle \exp\left(-\frac{F_{\rm in}\phi}{\delta f^2} - \frac{1}{2}F_{\rm in}q\right) \times \left(1 - \frac{\exp(F_{\rm in}q) - 1}{\exp(F^{\ddagger}q) - 1}\right) \right\rangle_{0<F_{\rm in}<F^{\ddagger}} \tag{4.6}$$

$$\text{where, } q \equiv \frac{2}{\delta f}\sqrt{\frac{2\phi}{F_{\alpha}^{\ddagger}} + \frac{\phi^2}{\delta f^2}}$$

Although the result of the Gaussian average and the derivative is too long to show here, it involves nothing more complicated then exponentials and error functions.

The total magnitude of the secondary relaxation peak is estimated by calculating the probability that fluctuations can stabilize a stringy reconfiguration for any size barrier less than $F_{\alpha}^{\ddagger}$. Integrating Γ over $F^{\ddagger}$ we get

$$\psi \approx \exp\left\{-\frac{2\phi\left(F_{\rm in} - \phi\right)}{\delta f^2}\right\} \tag{4.7}$$

The relative weight of the secondary relaxation peak increases with temperature as the dynamical crossover at $T_{\rm string}$ is approached, a trend that is validated experimentally[145]. At the crossover temperature and above, this secondary relaxation becomes the only remaining mode of activated relaxation. The sharp transition from activated to non-activated motions at T_c that is predicted by the non-fluctuating RFOT theory, as well as by mode coupling theory[9, 8] and the mean field theory of supercooled liquids[6, 97, 146], is therefore smoothed out by the string-like activated events made possible by fluctuations and exhibits no divergent critical behavior. This suggests that string-like secondary relaxations provide a mechanism for smoothly bridging the transition between mode coupling theory, valid above T_c and activated events described by RFOT theory, valid in the deeply supercooled regime below T_c[142]. In this temperature regime the secondary beta relaxations of mode coupling theory would be present and overlap in frequency with the string-like activated secondary relaxations, perhaps making the differentiation of the processes difficult.

The distribution of secondary relaxation free energy barriers Γ of equation 4.6 can be approximated by the Gumbel extreme value distribution function[147]. For $F^{\ddagger} > F_{\rm in}$ the barrier distribution decays exponentially as

$$\Gamma(F^{\ddagger} > F_{\rm in}) \sim \exp(-F^{\ddagger}q) \approx \exp\left(-2\frac{F^{\ddagger}\phi}{\delta f^2}\right) \tag{4.8}$$

The results agree with the sampled distribution of barriers for the string-like reconfiguration events alone (shown in figure 4.5). Using the fact that $\tau = \tau_0 \exp(F^{\ddagger}/k_B T)$ we see that equation 4.8 gives a power law distribution of relaxation times $P(\tau) \sim \tau^{-\gamma}$ where $\gamma \approx 2(s_c^{\rm string} - s_c)/\Delta C_P + 1$. Well above T_g the high barrier side of the secondary relaxation blends in with the primary relaxation peak. Thus the secondary relaxation from ramified reconfiguration events often appears as only a "wing" on the main distribution[148, 149]. However, when the decay exponent is large (i.e. near T_g or below) we expect the primary and secondary relaxation peaks to be sensibly distinct. As the temperature increases and approaches the string transition the decay exponent becomes small. In this limit the secondary relaxation peak, while growing in magnitude, will be seen to merge with the primary relaxation.

In the aging glass, the picture of secondary relaxation is slightly modified. If the liquid fell out of equilibrium at T_f then the frozen-in structure has an average excess energy per particle $\epsilon(T_f) = \epsilon(T_K) + \int_{T_K}^{T_f} dT \Delta C_P(T)$. At temperatures $T < T_f$ a region of the liquid undergoing reconfiguration would relax to a structure with average energy $\epsilon(T) < \epsilon(T_f)$. Thus the driving force for reconfiguration gains an energetic contribution and the configuration entropy in equation 4.1 is replaced by $Ts_c \rightarrow (Ts_c + \Delta\epsilon)$ where $\Delta\epsilon = \epsilon(T_f) - \epsilon(T) = \int_T^{T_f} dT' \Delta C_P(T')$. Lubchenko and Wolynes[22] have shown that this additional driving force results in a change in slope of the typical relaxation time as a function of temperature, and a transition to nearly Arrhenius behavior as the system falls out of equilibrium. Correspondingly, falling out of equilibrium causes the string tension to be reduced by an amount $\Delta\epsilon$, giving $\phi = Ts_c^{\rm string} - Ts_c - \Delta\epsilon$ and effectively makes the system appear closer to the dynamical crossover than an equilibrated system at the same temperature. Furthermore, the driving force fluctuations are frozen in as the aging glass falls out of equilibrium and become largely independent of temperature. These changes result in a broadening and flattening of the distribution of free energy barriers as the temperature is lowered, with the large free energy barrier decay given by

$$\Gamma(F^{\ddagger} > F_{\rm in}) \sim \exp\left(-2\frac{F^{\ddagger}(Ts_c^{\rm string} - Ts_c - \Delta\epsilon)}{T_f^2 k_B \Delta C_P(T_f)}\right). \tag{4.9}$$

The strength of the secondary relaxation in the aging regime becomes

$$\begin{aligned}\psi \approx \exp\Bigg\{ &- \frac{2(Ts_c^{\rm string} - Ts_c - \Delta\epsilon)}{T_f^2 k_B \Delta C_P(T_f)} \\ &\times \left(F_{\rm in} - (Ts_c^{\rm string} - Ts_c - \Delta\epsilon)\right)\Bigg\}.\end{aligned} \tag{4.10}$$

In the limit $T \to 0$ the distribution of barriers becomes largely independent of temperature with $\Gamma(F^{\ddagger} > F_{\rm in}) \sim exp(-\alpha F^{\ddagger})$ and $\alpha \approx ((z-2)v_{int}(T_f) - \Delta\epsilon)/(T_f k_B \Delta C_P(T_f))$. For a broad enough distribution of free energy barriers the dielectric absorption spectrum is determined through the simple relation, $\epsilon''(\omega) \sim P(F^{\ddagger} = -k_B T \ln \omega/\omega_0) \sim \omega^{\alpha T}$, and becomes essentially flat for low temperatures, resembling the so called constant loss spectrum. In a rejuvenating glass, an aged system that is heated to a temperature above T_f, the energetic contribution to the driving force is negative, $\Delta\epsilon < 0$. In this situation the system appears as if it is be further from the dynamical crossover temperature than an equilibrated system at the same temperature and secondary relaxations are relatively suppressed.

Nearly all glass forming liquids display secondary relaxations, dynamical modes seemingly distinct from the primary alpha relaxations. We have shown that by adding fluctuations to the existing structure of random first order transition theory a tail develops on the low free energy side of the activation barrier distribution which shares many of the features of the secondary relaxations observed in the laboratory. The relaxation process responsible for the tail differs from the primary relaxation mechanism in the geometry of the region undergoing cooperative reconfiguration. While primary relaxation takes place through activated events involving compact regions of the liquid, secondary relaxation is governed by more ramified string-like, or percolation-like clusters of particles. While the existence of secondary relaxation is nearly universal, the relevant motions are of shorter length scales than those for primary relaxation, allowing additional material dependent effects and, perhaps, less universal quantitative description than the main relaxation. The present theory, however, does suggests a universal mechanism for secondary relaxation. The

theory points out some important general trends about how these relaxations vary with temperature and substance which conform to observation. Fragile materials have larger fluctuations and should be more strongly affected by secondary relaxation than strong materials. Secondary relaxations grow in prominence with increasing temperature, merging with the primary relaxation peak and becoming dominant near the dynamical crossover temperature T_c. Finally the theory suggests that secondary relaxation can be viewed as a key component of the mechanism for smoothing what would otherwise be a very sharp transition between mode-coupling theory above T_c and activated events described by random first order transition theory below T_c.

Chapter 5

Constructing explicit magnetic analogies for the dynamics of glass forming liquids

The commonalities and contrasts between the glassy behavior of supercooled liquids and quenched disordered magnetic systems have been long studied. Both exhibit a diversity of long lived states with no apparent structural long range order. These states challenge the paradigms of standard many body physics. Starting in the 1980's, the disordered magnetic systems came under control, but only in mean field limit, through the concept of broken ergodicity using replica methods which allowed averaging over quenched disorder. Despite the absence of quenched disorder there is an analogy between the first order breaking of ergodicity predicted by mode coupling theory for structural glasses and the phase transition predicted for spin glasses that lack up-down symmetry (Potts spin glasses)[10, 26]. In mean field theory, the asymmetric spin glasses exhibit a Kauzmann entropy crisis[14] like that for supercooled liquids.

The analogy between glass forming liquids and mean field spin glasses is however incomplete. The observed dynamics of supercooled liquids fits the mean field mode coupling paradigm only modestly well[150]. The main problem with the mean field theory is its

neglect of important activated motions that allow a supercooled liquid to re-configure locally. The most convincing evidence for this is the near Arrhenius dynamics with large activation energy seen in structural glasses in the aging regime[138].

Activated motions have infinite barriers in mean field limit. Describing activated motions requires accounting for the finite interaction range. Accompanying a paucity of exact results[151], even the empirical situation remains controversial for finite range random magnetic systems[152, 153]. For the random field Ising magnet (RFIM), arguments based on renormalization group theory and droplet arguments do work well[154, 155, 20], but controversy remains as to the extent Ising spin glasses partake of mean field versus droplet features[156]. Nevertheless, useful analogies between glass forming liquids and disordered magnets have been drawn showing how droplet arguments give the Vogel-Fulcher law[19]. Similar arguments have also been adduced using replicas[14, 93, 157].

By applying density functional theory to determine the parameters in these droplet arguments[21] one predicts a large number of confirmed quantitative results for liquids[138]. The resulting random first order transition (RFOT) theory bears some resemblance to the nucleation picture of ordinary first order phase transitions. The theory's core is an analogy to the random field Ising magnet in a field. The average field in the magnet is related to the configurational entropy density of the liquid[19, 21]. Tarzia and Moore[158] suggest that supercooled liquids are related to Ising spin glasses in a field. When an average field is present, corresponding to a finite configurational entropy in the liquid, both the random field magnet and the spin glass have the same symmetry: neither model is expected to have a phase transition although this is still somewhat controversial[159]. While both magnetic analogies agree on this point, the activated dynamics in the two different analogical magnets differ because the interface energies in spin glass droplets have weaker scaling than the random field ferromagnet. To quantify this distinction in this paper we construct explicitly the analogy between a structural glass forming liquid and the corresponding short range disordered ferromagnet.

Replica methods along with liquid state theory allow an explicit mapping of the free energy landscape of a glass forming liquid onto a disordered Ising magnet. Using this explicit construction we may eschew droplet arguments entirely. Simulating the analogous magnet

shows the mapping reproduces, however, the main features of the RFOT analysis. The mean activation barrier and its fluctuations which give rise to non-exponential relaxation can be computed using importance sampling methods for the analog. Approximate arguments can place the analog system onto a phase diagram previously deduced for disordered magnets using renormalization group (RG). This construction suggests that under thermodynamic conditions when the mean field estimate for the configurational entropy would vanish, the liquid would still undergo a phase transition having one step replica symmetry breaking, despite the exact configurational entropy remaining non-zero[44, 160].

5.1 Theory

The analogy yields a description of a structural glass in terms of discrete spin-like variables tied to the liquid structure equilibrated at one time. A structural glass is statistically homogeneous but nonuniform with a density $\rho(\mathbf{x})$ that is not translationally invariant. Liquid state theory provides a free energy as a functional of such a density $\mathcal{F}[\rho(\mathbf{x})]$. While the complete equilibrium free energy $F = -k_B T \ln Z$ assumes all phase space can be sampled, close to the glass transition there is trapping in locally metastable states which manifests itself as extensively many local minima described by a configurational entropy density $S_c = \ln N_{ms}$. This non-ergodic behavior can be captured by a construction due to Monasson[161] in which an external random constraining pinning field couples m replicas of the system through an attractive potential. Each replica's density field is $\rho^k(\mathbf{x})$. The free energy of the m replica system is

$$F(m,\beta) = \lim_{g\to 0+}\Bigg[-\frac{1}{\beta m}\ln\int\prod_{k=1}^{m}\mathcal{D}\rho^k(\mathbf{x})\exp\Bigg\{ \\ -\beta\sum_k \mathcal{F}[\rho^k(\mathbf{x})] - \frac{g}{2m}\sum_{k,j,k<j}\int d\mathbf{x}[\rho^k(\mathbf{x})-\rho^j(\mathbf{x})]^2\Bigg\}\Bigg] \tag{5.1}$$

The typical free energy of a metastable frozen state, $\tilde{F} = \frac{\partial m F(m,\beta)}{\partial m}\big|_{m=1}$, differs from the complete equilibrium free energy by an amount $\delta F = \tilde{F} - F = \frac{\partial F(m,\beta)}{\partial m}\big|_{m=1} = TS_c$. In contrast to Monasson's thoroughly field theoretic formulation, we separate the m replicas

into one fiducial probe copy of particles interacting through the Hamiltonian $H(\{\mathbf{x}_i^f\}) = \sum_{i<j} u(\mathbf{x}_i^f - \mathbf{x}_j^f)$ and $m-1$ others described by density fields. Here u is the microscopic inter-particle potential. The pinning field on the other replicas is $\rho^f(\mathbf{x}) = \sum_i \delta(\mathbf{x} - \mathbf{x}_i^f)$. We can write:

$$F(m,\beta) = -\lim_{g\to 0}\frac{1}{\beta m}\ln\int \mathcal{D}\{\mathbf{x}_i^f\}e^{-\beta H\left(\{\mathbf{x}_i^f\}\right)}\int\prod_{k=1}^{m-1}\mathcal{D}\rho^k(\mathbf{x})\exp\Bigg\{-\beta\sum_{k=1}^{m-1}\mathcal{F}[\rho^k(\mathbf{x})] - \frac{g}{2m}\sum_{k=1}^{m-1}\int d\mathbf{x}[\rho^k(\mathbf{x})-\rho^f(\mathbf{x})]^2 - \frac{g}{2m}\sum_{k=1}^{m-1}\sum_{j=1,k<j}^{m-1}\int d\mathbf{x}[\rho^k(\mathbf{x})-\rho^j(\mathbf{x})]^2\Bigg\} \tag{5.2}$$

In calculating the free energy with respect to the probe replica we ignore peripheral interactions not involving the probe, thus decoupling the partition function

$$F(m,\beta) = -\lim_{g\to 0}\frac{1}{\beta m}\ln\int \mathcal{D}\{\mathbf{x}_i^f\}e^{-\beta\mathcal{H}\left(\{\mathbf{x}_i^f\}\right)}[Z_q]^{m-1} \tag{5.3}$$

such that each replica is constrained by a potential to the vicinity of the fiducial copy:

$$Z_q = \int\mathcal{D}\rho(\mathbf{x})\exp\Bigg\{-\beta\mathcal{F}[\rho(\mathbf{x})] - \frac{g}{2m}\int d\mathbf{x}[\rho(\mathbf{x})-\rho^f(\mathbf{x})]^2\Bigg\} \tag{5.4}$$

For a glassy system, when $TS_c = \frac{\partial F(m,\beta)}{\partial m}|_{m=1}$ is finite, in the limit $m \to 1$, the replicated free energy is dominated by a saddle point corresponding to the spontaneous ordering of replicas in phase space. The saddle point solution to the free energy is found by minimizing the exponential's argument.

$$\frac{\delta}{\delta\rho(\mathbf{x})}\left[\beta\mathcal{F}[\rho(\mathbf{x})] + \frac{g}{2m}\int d\mathbf{x}[\rho(\mathbf{x})-\rho^f(\mathbf{x})]^2\right]_{\rho=\tilde{\rho}} = 0 \tag{5.5}$$

The free energy functional can be written, à la density functional theory, as the sum of an entropic cost to localize the density and an interaction term.

$$\beta\mathcal{F}[\rho(\mathbf{x})] \approx \int d\mathbf{x}\rho(\mathbf{x})\ln\rho(\mathbf{x}) + \beta F_{int}[\rho(\mathbf{x})]. \tag{5.6}$$

While the free energy functional $\mathcal{F}[\rho]$ is globally minimized by a uniform equilibrium solution with mean density ρ_0, $\mathcal{F}[\rho]$ also has local minima corresponding to frozen aperiodic densities. The g coupling, even as g vanishes, picks out one particular minimum around the structural state ρ^f. Thus $\mathcal{F}[\rho]$ can be analyzed in terms of the similarity, or overlap $q = \int d\mathbf{x}(\rho(\mathbf{x}) - \rho_0)(\rho^f(\mathbf{x}) - \rho_0)$, between $\rho(\mathbf{x})$ and $\rho^f(\mathbf{x}) = \sum_i \delta(\mathbf{x} - \mathbf{x}_i^f)$. A schematic of the free energy as a function of the order parameter q as computed in references [6] and [93] is shown in figure 5.1a. The free energy difference between the large overlap solution and the small overlap solution is the excess free energy of the frozen glass over the equilibrium free energy and is determined by TS_c.

The large overlap state is well approximated by a density distribution of a sum of Gaussians centered around the particle locations of the fiducial (probe) copy $\rho(\mathbf{x}) = \sum_i \rho_i(\mathbf{x}) = \sum_i \left(\frac{\alpha_i}{\pi}\right)^{3/2} e^{-\alpha_i(\mathbf{x}-\mathbf{x}_i^f)^2}$. The localization parameters, $\{\alpha_i\}$, determine the local overlap. Near the large overlap minimum, $q\big(\alpha_i \gg \rho_0^{2/3}\big) = \sum_i \left((\alpha_i/\pi)^{3/2} - \rho_0\right)$. In the opposite limit, near the global free energy minimum, the density ansatz reduces to the mean density and $q(\{\alpha_i\} \to 0) = 0$.

For large values of $\{\alpha_i\}$ the particles are localized very near the fiducial locations $\{\mathbf{x}_i^f\}$ and F can be evaluated by using the independent oscillator approximation[162, 7] which decouples the particles at the individual site level. Within this approximation F_{int} can be expressed as a sum of effective potentials between the interacting density clouds, $\beta V_{eff}\left(|\mathbf{x}_i^f - \mathbf{x}_j^f|;\alpha_j\right) \equiv -\ln\int d\mathbf{x}_j\rho_j(\mathbf{x}_j)e^{-\frac{1}{2}\beta u(\mathbf{x}_i^f - \mathbf{x}_j)}$.

$$\begin{aligned}\beta F_{glass}\Big(\{\mathbf{x}_i^f\},\{\alpha_i\}\Big) = &\sum_i \frac{3}{2}\ln\frac{\alpha_i\Lambda^2}{\pi e} \\ &+ \sum_{ij}\beta V_{eff}\left(|\mathbf{x}_i^f - \mathbf{x}_j^f|;\alpha_j\right).\end{aligned} \tag{5.7}$$

The localization parameters corresponding to the large overlap solution, $\{\alpha_i^{\uparrow}\}$, can be found by applying a self consistency condition[162, 7]. The existence of the free energy minimum at large overlap reflects the cage effect where the motion of a particle is restricted

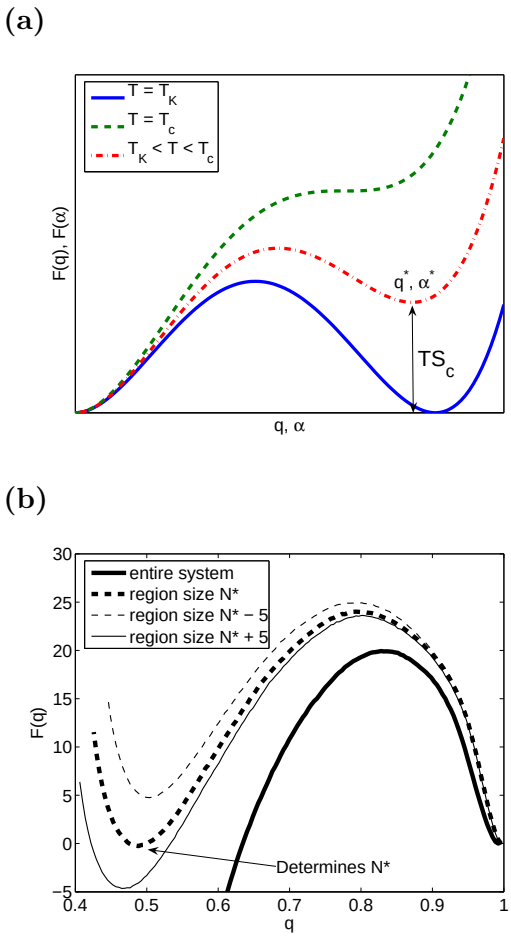

Figure 5.1: (a) Schematic mean field free energy profiles for supercooled liquids at the dynamical crossover temperature (dashed line), the Kauzmann temperature (solid line), and an intermediate temperature (dot-dashed line). In mean field the particle localization, α, and the structural overlap, q, are equivalent reaction coordinates. The secondary free energy minimum at $T_K < T < T_c$ demonstrates the existence of metastable structural states in supercooled liquids. (b) Free energy profiles calculated for the finite range Ising magnet analogous to the LJ liquid. The minimum size needed to escape the free energy minimum and thus reconfigure the liquid at $s_c = 1.10$ is $N^* = 148$ particles.

by its neighbors. To first order one may compute the potential $\beta V_e\left(\mathbf{x}_i - \mathbf{x}_i^f, \{\alpha_j\}\right) \equiv \sum_j \beta V_{eff}\left(|\mathbf{x}_i - \mathbf{x}_j^f|; \alpha_j\right)$ and expand around small displacements of particle i, $w_i = |\mathbf{x}_i - \mathbf{x}_i^f|$.

$$\beta V_e\left(w_i, \{\alpha_j^{\uparrow}\}\right) \approx \beta V_e|_{w_i=0} + w_i^2 \frac{1}{6}\nabla^2 \beta\, V_e|_{w_i=0} \tag{5.8}$$

$$\beta V_e\left(w_i, \{\alpha_j^{\uparrow}\}\right) \approx \beta\, V_e|_{w_i=0} + \alpha_i^{\uparrow} w_i^2 \tag{5.9}$$

The linear term gives no contribution because the fiducial replica becomes centered on a stationary location with all forces canceling. The localization parameter of particle i thus can be computed from the curvature of the effective potential, $\alpha_i^{\uparrow} = \frac{1}{6}\nabla^2 \beta V_e\left(|\mathbf{x}_i - \mathbf{x}_i^f| = 0, \{\alpha_j^{\uparrow}\}\right)$, giving a self-consistent solution for $\alpha_i^{\uparrow}$[28, 7].

Near the uniformly low overlap state the interaction free energy F_{int} follows from the equilibrium liquid equation of state, $Z_{EoS}(\eta)$, where η is the packing fraction[163]:

$$F_{liq}^{\downarrow} = N \ln \rho_0 \Lambda^3 - N + N \int_0^{\eta} (Z_{EoS} - 1) \frac{d\eta'}{\eta'}. \tag{5.10}$$

To characterize the reconfiguration events and develop the magnetic analogy one must also examine non-uniform solutions. At the interface between the two solutions there must be some energetic penalty due to the patching together of distinct configurational states. At an interface, one particle is in the large overlap state while it's neighbor has small overlap, so the pair interaction becomes $\beta V_2^{eff}\left(|\mathbf{x}_i^f - \mathbf{x}_j^f|; \alpha_i^{\downarrow}, \alpha_j^{\uparrow}\right) = -\ln \int d\mathbf{x}_i d\mathbf{x}_j \rho_i^{\downarrow}(\mathbf{x}_i)\rho_j^{\uparrow}(\mathbf{x}_j) e^{-\frac{1}{2}\beta u(\mathbf{x}_i - \mathbf{x}_j)}$. The small overlap parameters $\{\alpha_i^{\downarrow}\}$ determine $\rho_i^{\downarrow}$ and are obtained in the self-consistent phonon theory by matching the entropy of the low overlap state calculated within the Gaussian density ansatz with the entropic term of the equilibrated liquid:

$$\sum_i \frac{3}{2} \ln \frac{\alpha_i^{\downarrow} \Lambda^2}{\pi e} = N \ln \rho_0 \Lambda^3. \tag{5.11}$$

For any combination of the discrete values of $\{\alpha_i^{\downarrow}\}$ and $\{\alpha_i^{\uparrow}\}$, the free energy of the supercooled liquid is equivalent to a pairwise interacting model with spins located at

the fiducial locations, $\{\mathbf{x}_i^f\}$.

$$\beta H = -\sum_i h_i(1-s_i) + \sum_{i<j} J_{ij}\left[s_i(1-s_j) + s_j(1-s_i)\right], \tag{5.12}$$

where the spin, $s_i = 1$, corresponds with large overlap and $s_i = 0$ small overlap at a site. The average field is found from the bulk free energy difference between the states, $\sum_i h_i = \beta F_{glass} - \beta F_{liq} = N s_c/k_B$, with a heterogeneous local configurational entropy resulting from the alpha variations.

$$h_i = \frac{3}{2}\ln\frac{\alpha_i^{\uparrow}}{\pi} + \beta\sum_j V_{eff}(|\mathbf{x}_i^f - \mathbf{x}_j^f|;\alpha_j^{\uparrow}) - \frac{1}{N}F_{liq} \tag{5.13}$$

The interactions defined through the effective potential give the surface energies of droplets within the RFOT picture and are explicitly

$$J_{ij} = V_2^{eff}\left(|\mathbf{x}_i^f - \mathbf{x}_j^f|;\alpha_i^{\downarrow},\alpha_j^{\uparrow}\right) + V_2^{eff}\left(|\mathbf{x}_i^f - \mathbf{x}_j^f|;\alpha_i^{\uparrow},\alpha_j^{\downarrow}\right). \tag{5.14}$$

5.2 Application to a simulated glass

The mapping to the disordered Ising model should be carried out for each fiducial equilibrium liquid structure. We sample fiducial structures of the Kob-Andersen 80-20 mixture of two types of Lennard-Jones (LJ) particles at density 1.2 (in LJ reduced units). The pairs have interaction parameters[165, 163], $\sigma_{AA} = 1.0$, $\sigma_{BB} = 0.8$, $\sigma_{AB} = 0.88$, $\epsilon_{AA} = 1.0$, $\epsilon_{BB} = 1.5$, $\epsilon_{AB} = 0.5$. The fiducial structures were obtained by simulated annealing runs to the temperature $T_{MD} = 0.45$. The equilibration time for these simulations reaches a tenth of a microsecond when referenced to argon.

The parameters $\{\alpha_i^{\uparrow}\}$ ($\{q_i^{\uparrow}\}$) and $\{\alpha_i^{\downarrow}\}$ ($\{q_i^{\downarrow}\}$) are calculated for every particle. The mean RMS deviation determined from $\{\alpha_i\}$ is about 0.12 particle spacings, rather close to the Lindemann parameter expected for periodic crystals $d_L \approx 0.1$ independent of the force law. The RMS actually observed during the MD run at $T_{MD} = 0.45$ is consistent with this estimate $d_L = 0.113$.

The distribution of calculated interactions is shown in figure 5.2a. The interaction free energy per neighbor is $J_i \equiv \frac{1}{z_i}\sum_j J_{ij}$ where z_i is the number of neighbors of particle i. The typical interaction $\bar{J} \equiv \frac{1}{N}\sum_i J_i$ is directly related to σ, the mismatch free energy penalty in RFOT theory for a particle at a flat interface between regions of high and low overlap. In the Ising mapping $\beta\sigma_I = n_{bb}\bar{J}$ where $n_{bb} = 3.2$ is the typical number of bonds broken by the interface. The direct calculation yields $\bar{J} = 0.55$ giving $\beta\sigma_I = 1.77$ not very different from the RFOT theory estimate usually used[98] $\sigma_{RFOT} = \frac{3}{4}k_BT\ln\frac{1}{d_L^2\pi e} = 1.85k_BT$.

In RFOT theory the configurational entropy parametrizes a liquid's descent into the glassy regime. In harmony with many experimental observations[140, 22, 123], the dynamic crossover and the laboratory glass transition occur at universal critical entropies of $s_c(T_c) = 1.12k_B$ and $s_c(T_g) = 0.82k_B$, respectively.

Because of the rapidly increasing equilibration time scales it is impossible presently to obtain proper fiducial structures directly at very low temperatures via molecular dynamics. We can, however, treat the configurational entropy, and therefore the average field, as variable in order to extrapolate to find the magnetic system analogous to a liquid equilibrated at a much lower temperature, eventually extrapolating all the way to the ideal glass transition by taking $\bar{h} = \frac{1}{N}\sum_i h_i \to 0$. The presence of even a small average field is thought to destroy the phase transitions of both spin glasses and the random field Ising magnets, but at zero field a transition to a phase with long range correlations can still occur. Would a transition occur for the liquid analog when $\bar{h} = 0$, i.e. when the mean field configurational entropy vanishes? We answer this by appealing to an RG analysis of Migliorini and Berker[164] for the phase diagram for an Ising system in which both the fields and the interactions fluctuate randomly and independently, encompassing both the RFIM and the short range spin glasses. Their model is on a cubic lattice. We present their phase diagram in figure 5.3 in terms of the mean field theory based normalization where both the field fluctuations, δh, and the fluctuations of the interaction strength, $\delta J z^{1/2}$, are normalized by the total interaction energy per site $\bar{J}z$. This parametrization should eliminate trivial near neighbor lattice dependence. This zero average field phase diagram is shown at a temperature $T = 1$ coinciding with the established temperature of the analogous magnet.

The results for the simulated Kob-Andersen liquid are indicated by the dot suggesting the disorder in both the fields and the interactions is sufficiently modest so that the system would undergo a phase transition to a state with infinite correlation lengths and divergent relaxation times when the field vanishes. This extrapolation implies the Kob-Andersen LJ liquid should possess a true phase transition to a state with one step replica symmetry breaking (RSB), even though the re-normalized configurational entropy, which would include small scale droplet excitations, strictly speaking remains finite. For such a broken replica symmetry state the free energy landscape has divergent barriers between a finite number of collective free energy basins each one of which still has finite configurational entropy due to local defects.

According to Landau, the excess heat capacity[166] yields $\delta s_c = \sqrt{\Delta C_p k_B / N_{corr}}$, where N_{corr} is the volume within which the disorder is correlated. The explicit mapping for the LJ system gives entropy fluctuations $\delta h = \delta s_c / k_B = 0.38$, smaller than a typical fragile glass forming liquid such as ortho-terphenyl (OTP). Assuming a similar distribution of interactions but rescaling the field fluctuations to that calculated for ortho-terphenyl yields the triangular position on the RG phase diagram of figure 5.3 while the square mark indicates where the strong glass forming liquid GeO_2 would lie. Even though OTP is rather fragile, we see it would still be expected to obey one step RSB.

Our extrapolations neglect any structural changes that occur in an actual fluid upon cooling yet we can test how well the direct dynamics of the extrapolated analog model correspond to droplet analysis. Escape from the metastable ($s = 1$) large overlap state corresponds with a large scale activated, structural rearrangement of the liquid. Directly simulated escape times are shown as circles in figure 5.4a. The relaxation time grows rapidly at the dynamical crossover temperature appearing to diverge as $s_c, \bar{h} \to 0$. Below the dynamic crossover the growth in relaxation time is well fit by $\ln \tau/\tau_0 \sim s_c^{-\psi}$. The proportionality constant for the inverse linear fit ($\psi = 1$) is $22 k_B$, while droplet arguments in RFOT theory predict a slightly larger value $\ln \tau/\tau_0 = 32 k_B/s_c$. $\psi = 2$, corresponding to the unwetted result from RFOT theory[21], actually gives a closer fit to the relaxation time curve. This is consistent with what we have already seen in figure 5.3, that the analog magnet underestimates the disorder in the field moving the system away from the critical

line where wetting is dominant.

The average overlap of the liquid frozen density fields maps onto the magnetization in the analog magnet, $q = \frac{1}{N}\sum_i s_i$. This coordinate can be used to monitor escape from local minima. We create free energy profiles for this local collective reaction coordinate using the weighted histogram analysis method[167, 168, 169] (WHAM). The resulting free energy profile, calculated with $\bar{h} = s_c/k_B = 1.1$, is shown as a thick solid line in figure 5.1b. The metastable minimum at large overlap is separated from the global minimum at small overlap by a free energy barrier that accounts for the relaxation time according to $\tau = \tau_0 e^{\beta F^\ddagger}$.

The global overlap is not an ideal reaction coordinate for reconfiguration, as it averages over reconfiguration events occurring at spatially distinct regions. By selecting a spherical region at random and only permitting motion within that region, the overlap becomes a good reaction coordinate. This is the magnetic analogy of the landscape "library construction"[22] and is similar to a technique recently used to calculate the surface tension near a first order transition[170]. By varying the region size, the minimum size to irreversibly escape a minimum and reconfigure the liquid, N^*, can be determined. Free energy profiles for several region sizes around N^* are shown in figure 5.1b. The free energy barriers computed for regions of size N^*, converted to relaxation time, are shown in figure 5.4a. Using WHAM and the library construction allows descent much further into the glassy regime than is possible via direct simulation. The predicted minimum reconfiguration size is shown in figure 5.4b. At high temperatures, $s_c > 1$, the growth of region size with decreasing s_c is consistent with $N^* \propto s_c^{-2}$ expected from RFOT theory, but at low temperatures the growth falls off as the result of finite size effects since the cluster size approaches the simulated system size itself. The free energy barrier is also underestimated for the low temperature range.

Not all cooperatively rearranging regions are created equal. The resulting dynamic heterogeneity of the liquid is seen in figure 5.5 showing a collection of free energy profiles for different regions at $\bar{h} = s_c/k_B = 1.1$. There is clearly a spread of relaxation times which can give rise to the stretched exponential relaxation behavior $\phi(t) = e^{-(t/\tau)^{\beta_{KWW}}}$ common to glassy systems. If the relaxation is entirely heterogeneous the stretching exponent, β_{KWW},

was shown in reference [98] to be related to the spread of free energy barriers, $\delta F^{\ddagger}$, through the relation $\beta_{KWW} \approx \left(1 + (\delta F^{\ddagger}/k_B T)^2\right)^{-1/2}$. Xia and Wolynes argued that regions do not reconfigure completely independently, so free energy barriers larger than the mean are lowered by facilitation effects of neighboring regions. Using the barrier distribution corrected in this way for facilitation yields a non-exponentiality parameter nearly independent of temperature, $\beta_{KWW} \approx 0.6$, a value characteristic for fragile liquids.

5.3 Conclusion

Using a mixed density functional/atomistic replica formalism, the dynamics of the structural glass forming liquids can be mapped onto a general disordered Ising model. This mapping allows a computationally inexpensive route to low temperature dynamics impossible currently by direct simulation. Using this information from the replica density functional one can guide molecular dynamics simulations carried out at complete atomic detail to more easily reach low temperature structural states.

Our results suggest the Kob-Andersen liquid should demonstrate one step replica symmetry breaking at a sufficiently low temperature even though its configurational entropy including local droplet excitations, strictly speaking, will not vanish. The system is, in this sense, closer to the random field Ising magnet than it is to the Edwards Anderson short range spin glass model. The results from the simulation are consistent with droplet based predictions using the existing random first order transition theory estimates.

Chapter 5, in full, is a reprint of the material as it appears in the Journal of Chemical Physics 129 194505 (2008), J. D. Stevenson, A. M. Walczak, R. Hall, and P. G. Wolynes. The dissertation author was the primary investigator and author of this paper.

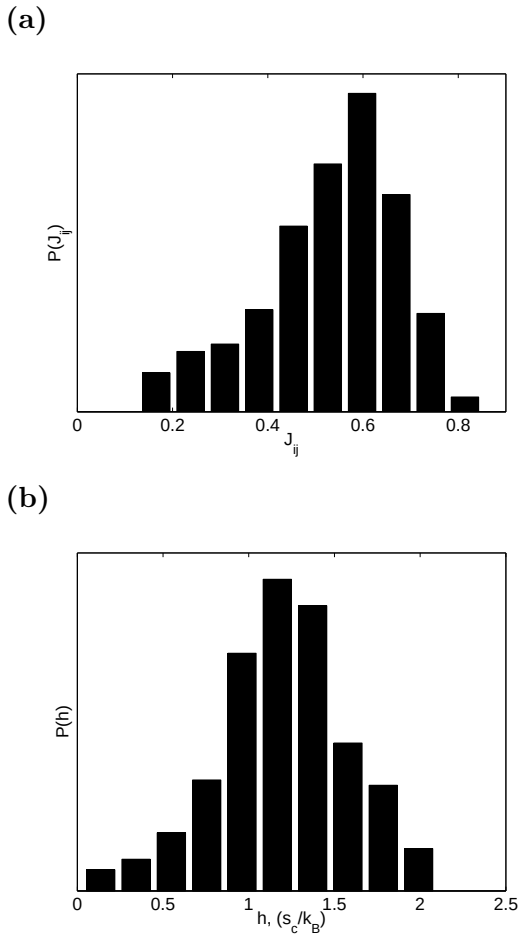

Figure 5.2: The distributions of interactions and local fields of the magnet analogous to the simulated LJ two compound glass. In this mapping $\bar{h}$ is directly related to the configurational entropy, $\bar{h} = s_c/k_B$. The fields are shown at $\bar{h} = 1.2$, close to the dynamical crossover temperature.

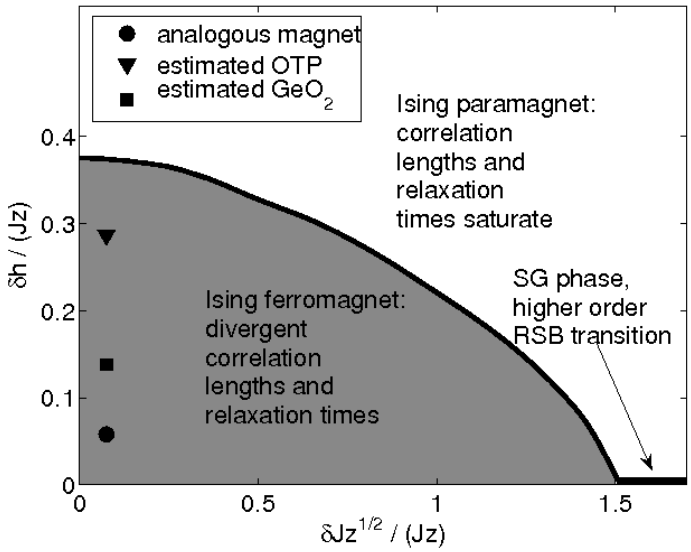

Figure 5.3: Phase diagram of the Ising model with random bonds and fields adapted from reference [164]. The parameters calculated for the magnet analogous to the LJ liquid (circular mark) indicate that the liquid would undergo a true phase transition at the ideal glass transition. The triangular and square marks indicate estimates of where the glass forming liquids OTP and GeO_2 would fall on the phase diagram.

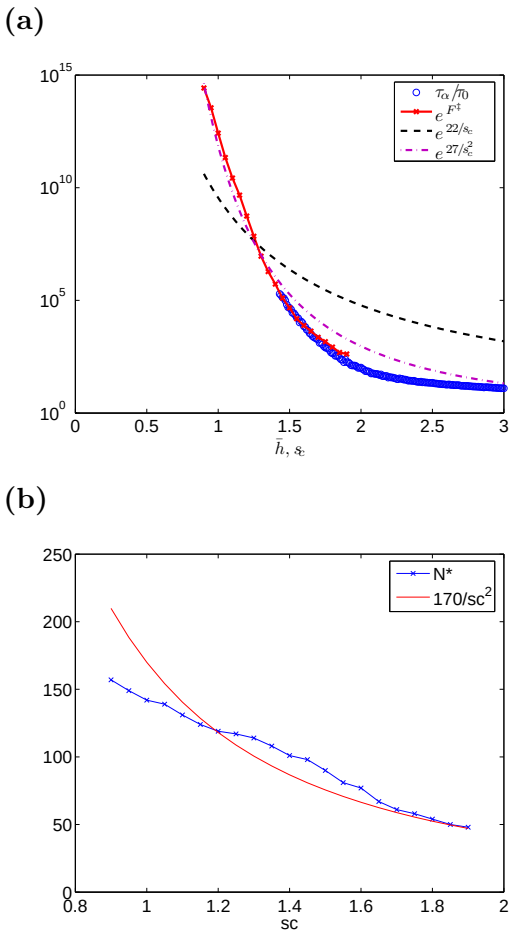

Figure 5.4: (color online) (a) Relaxation times of the Ising model analogous to the LJ liquid (circles). The solid line gives relaxation times calculated from free energy barriers. The dashed lines show fits using relations derived in RFOT theory (see text). (b) The minimum region size able to irreversibly reconfigure.

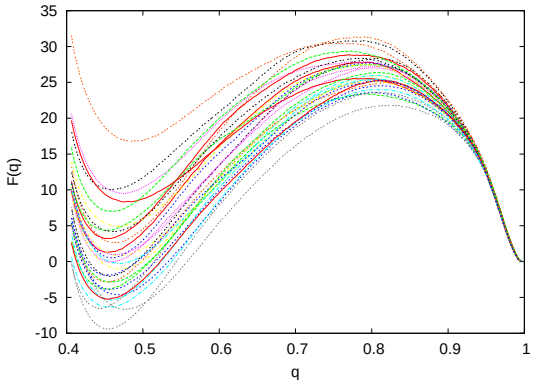

Figure 5.5: (color online) Free energy profiles for different regions at $\bar{h} = s_c/k_B = 1.1$. The distribution of free energy barriers gives rise to the stretched exponential relaxation behavior common to glassy systems.

Chapter 6

On the surface of glasses

Paying attention to the properties of interfaces has, since the time of Van der Waals, helped to clarify our understanding of bulk phase transitions[171]. Studying the mobility at the surface of glasses and supercooled liquids has the potential to be equally enlightening about the glass transition[172, 173]. Theories of the glass transition predict a growing length scale of correlated dynamics as the glass transition is approached[138, 174, 175, 110]. This growth, according to the most successful theories, is quite modest. It has only in recent years been widely acknowledged that there is such a slowly growing length scale in bulk glasses[23, 16]. The dynamics of a glass or supercooled liquid should be perturbed within a few correlation lengths of its surface. Many experiments do show significant perturbations of the glassy dynamics at free surfaces or in confined spaces[176]. The picture that emerges from these experiments is, at present, still somewhat confused. In general, mobility seems to be increased at a free surface, although sometimes a diminished mobility has been observed. At interfaces with solids both increases and decreases in mobility have been reported[177, 178]. It seems likely that this complex set of behaviors reflects the fact that the dynamics of the liquid can be strongly influenced by the liquid's static structure which also will be perturbed by the interface — in the extremes, partial crystallization can occur at a free interface while a drying layer may sometimes insulate a confined fluid from its solid surroundings. While noting these complications, we feel it is nevertheless worth-

while to present a simplified view of glass and supercooled liquid surfaces in the context of the random first order transition theory of the glass transition.

The random first order transition (RFOT) theory is a constructive approach to structural glass dynamics that has explained quantitatively numerous bulk glass phenomena[138]. It was recognized very early on that growing length scales should be associated with an ideal glass transition as envisaged in RFOT theory[19, 14]. Indeed some of the early experiments on confined supercooled liquids carried out by Jonas[179] were motivated by a desire to test these expectations. It turns out present day RFOT theory for molecular liquids can make somewhat more definite predictions than was done in those early days, at least for an idealized interface which can be taken to have no change in static structure from the bulk. We show for this idealization that the maximum mobility at a completely free interface is related in a very simple way to the bulk mobility. In terms of relaxation times, the RFOT result for the surface relaxation time is simply $\tau_{surf} = \sqrt{\tau_0 \tau_{bulk}}$. We also show that RFOT theory suggests that as measured by an effective local glass transition temperature T_g^{local} the influence of the interface can appear to be rather far-reaching into the bulk, consistent with some experiments.

At the smallest length scales the dynamic arrest of glasses results from the cage effect in which a particle's motion is constrained by the presence of its neighbors. In mean field theory this leads to a friction crisis at the mode coupling theory (MCT) critical temperature and the emergence of an ensemble of aperiodic crystal structures having an extensive configurational entropy s_c per particle. Below the dynamical transition at T_c any large scale motion that takes place is necessarily collaborative. Near a free surface this picture is modified. Since surface particles feel a weaker structural cage, essentially only on the inner side, they would go through a dynamic arrest at a lower temperature and remain more mobile below the bulk glass transition temperature. The collaborative dynamics propagates the enhanced mobility at the surface some distance into the bulk. This depth would be determined by the length scale of cooperativity.

In the mean field limit (made precise in Kac models by Franz[180]) two cooperative length scales can be defined for random first order transition theory[14]. One scale, ξ_{MCT}, is directly related to the dynamical transition at T_c which resembles a spinodal[110], the

other is related to the size of regions that rearrange by activated motions and scales with the configurational entropy s_c[21]. The latter scale diverges at the Kauzmann temperature with an exponent $\xi_{RFOT} \sim a s_c^{-2/3}$. Within the sharp, thin wall approximation the RFOT theory yields a numerical coefficient a that appears consistent with experimental values for molecular glasses[21]. The scaling exponent used to fit inferred lengths from χ_4 is also not inconsistent with RFOT theory, although a larger value provides a better fit[23, 16]. For molecular liquids governed by short range interactions the dynamical (mode coupling) length would not actually diverge at T_c because of a dynamical cutoff from the activated events and will not be too different from ξ_{RFOT}.

We first review the theory of bulk activated dynamics[138]. Below the mode coupling theory (MCT) transition, dynamics takes place on a rugged free energy landscape[14, 28, 6]. Particle motion occurs locally through transitional hops between metastable structural states which resemble, in many ways, nucleation processes between different aperiodic crystal structures[21, 14]. The magnitude of the free energy barrier can be found by a competition between the entropic cost of remaining confined to one minimum free energy structure and a mismatch free energy penalty, σ, for having two mean field solutions adjacent to each other but in distinct structural states. The free energy profile governing nucleation of a spherical cooperative region of radius r is

$$F_{bulk}(r) = 4\pi r^2 (r_0/r)^{1/2} \sigma_0 - \frac{4}{3}\pi r^3 n_0 T s_c \tag{6.1}$$

The surface penalty $\sigma(r) = (r_0/r)^{1/2}\sigma_0$ scales with r due to renormalization effects of wetting by the diverse set of structures[21, 20]. There is some discussion in the community about the value of the surface scaling exponent[16, 15]. In the absence of wetting or when it is incomplete, a weaker variation of $\sigma(r)$ is expected. In any event, at short length scales σ_0 can be obtained from a crude density functional calculation giving $\sigma_0 = \frac{3}{4} k_B T r_0^{-2} \ln \frac{1}{d_L^2 \pi e}$ where $d_L \approx 0.1$ particle spacings is the Lindemann length, and $n_0 = r_0^{-3}$ is the density of the liquid. The configurational entropy, s_c, measures the number of available structural states. The resulting free energy barrier for reconfiguration events in bulk, assuming wetting, is

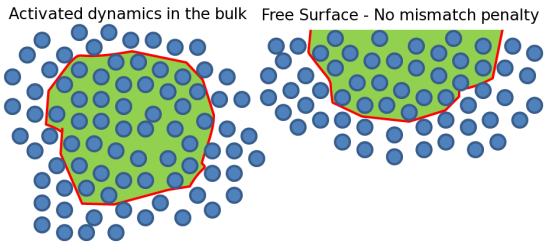

Figure 6.1: (Color online) In the bulk, at low temperatures, activated motion occurs within roughly spherical regions. Near a free surface a rearranging hemispherical region feels no mismatch penalty on interface along the free surface leading to much faster dynamics than the bulk.

$$F^{\ddagger}_{bulk} = \frac{3\pi\sigma_0^2 r_0^4}{T s_c(T)} \tag{6.2}$$

The relaxation time $\tau_\alpha = \tau_0 e^{F^{\ddagger}/k_B T}$ diverges at the Kauzmann temperature ($s_c(T_K) \to 0$) and thus follows the Vogel-Fulcher behavior in the deeply supercooled region $\tau_\alpha \sim e^{B/(T-T_K)}$. The length scale of an activated event follows from balancing the terms in the free energy profile

$$r^* = r_0 \left(\frac{3\sigma_0 r_0^2}{T s_c(T)} \right)^{2/3} \tag{6.3}$$

This length scale increases with decreasing temperature, reaching a universal value of about 5 inter-particle spacings at the glass transition temperature corresponding to a one hour relaxation time.

The RFOT analysis of bulk activated dynamics can be easily modified (see figure 6.1) to treat motions near a free surface. Near a completely free surface with no structural modifications, the transition state would rearrange a region of hemispherical shape in order to minimize the surface area subject to the mismatch penalty[1]. The flat face of the hemisphere lies along the free surface and is assumed not to contribute to the mismatch penalty. The free energy profile for the hemispherical rearranging region becomes

[1]For shapes other than hemispheres the wetting effect would need to be modified to correctly deal with the curvature, but the hemisphere, or something close to it, would still be the most favored shape.

$$F_{surf}(r) = 2\pi r^2 (r_0/r)^{1/2}\sigma_0 - \frac{2}{3}\pi r^3 n_0 T s_c. \tag{6.4}$$

Since both terms in the expression are halved from the equation for bulk dynamics we see that the size corresponding to the transition state for activated rearrangement remains unchanged from that for the bulk, but the resulting free energy barrier is reduced by a factor of 2,

$$F^{\ddagger}_{surf} = \frac{1}{2}\frac{3\pi\sigma_0^2 r_0^4}{T s_c(T)} \tag{6.5}$$

This seemingly innocuous change leads to dramatically faster relaxation at free surfaces than occurs in the bulk. Molecular motion near the surface of a glass would still be detectable even if the bulk were essentially frozen. We see that very near the surface, the relaxation time is related very simply to the bulk value,

$$\tau_{surf} = \sqrt{\tau_0 \tau_{bulk}}. \tag{6.6}$$

This result is independent of the wetting.

According to RFOT, on laboratory time scales, the ideal surface layer will be able to "hike" (using the colorful expression of Ediger[1]) much further down the free energy landscape than the bulk, reaching lower energy, more stable configurations than the bulk is likely to find. The surface motion will freeze out, i.e. go through its own glass transition (T_g^{surf}) only when τ_{surf} becomes larger than the laboratory time scale. For the same laboratory time scale, according to equation 6.5 this will happen when the configurational entropy is half the characteristic configurational entropy of the bulk glass transition. The bulk glass transition entropy is very nearly material independent[45, 24], and likewise the free surface glass transition will occur at a characteristic *bulk* entropy value. For a one hour time scale this characteristic entropy is

$$s_c(T_g^{surf}) = \frac{1}{2} s_c(T_g^{bulk}) \approx 0.41 k_B \tag{6.7}$$

Ediger and co-workers[1] have recently shown how to construct a macroscopic glass sample via vapor deposition reaching much lower in the energy landscape than was possible

by the usual bulk cooling of a liquid. They argue this ultra-stable glass arises from the free surface's excess mobility. For slow deposition on a cold substrate the growing glass, owing to the higher mobility, can more thoroughly rearrange near the free surface to form exceedingly stable structures. They assign a fictive temperature to their sample, T_f, defined as the temperature where a glass of similar stability, but created by bulk cooling would fall out of equilibrium. T_f can be used to measure the sample's position on the free energy landscape relative to an ordinary glass through the parameter,

$$\theta_K = \frac{T_g - T_f}{T_g - T_K} \tag{6.8}$$

This parameter increases with the stability of the glass, reaching one for an ideal glass. In principle if there were in fact no entropy crisis, θ_K could exceed one. θ_K can be parametrized by the configuration entropy, an equivalent measure of structural stability. Using the linear extrapolation vanishing at T_K valid for low temperature ($T < T_g$) the RFOT free surface mobility would yield for a rate of deposition equal to one correlation length per hour

$$\theta_K = 1 - \frac{s_c(T_f)}{s_c(T_g)} \leq \frac{1}{2} \tag{6.9}$$

As the enhanced surface mobility freezes out at T_g^{surf}, this temperature should be seen as a limiting value for T_f leading to the inequality above. Ediger's experiments yielded $\theta_K \approx 0.4$ for both liquids studied[1]. It would take about 10^5 years to to make these highly stable glasses via traditional bulk cooling, while roughly the age of the universe would be required for a glass with $\theta_K = 1/2$. Unless the surface structure is greatly modified leading to a locally smaller T_K, vapor deposition should not yield glasses with stability much greater than the naive RFOT limiting value.

The linear extrapolation for $s_c(T)$ is valid near T_K, but for some liquids at higher temperatures a better approximation is[60] $s_c = s_\infty(1 - T_K/T)$. Recognizing this feature does add some material dependence to the limiting stability

$$\theta_K \leq \frac{T_g}{T_g + T_K}. \tag{6.10}$$

Fragile liquids still have a limit near 1/2, but strong liquids have the possibility of descending further in terms of temperature (but *not* in terms of configurational entropy) than fragile liquids. The fragilities for the two glasses so far studied by Ediger are similar and would yield $\theta_K \leq 0.57$(IMC) and $\theta_K \leq 0.58$(TNB) for the nanometer per hour deposition rate.

A key prediction of this analysis is that the fictive temperature is a function of the logarithm of the deposition rate. More precisely the configurational entropy at the fictive temperature is a universal function of the logarithmic deposition rate. The limiting stability given above assumes a deposition rate of one correlation length per hour. More generally, for a deposition rate k the mobile surface layer of depth ξ will be equilibrated on a time scale ξ/k, which is related to the fictive temperature through the relationship $\xi/k = \tau_0 e^{F^{\ddagger}(T_f)/k_B T_f} = \tau_0 e^{A_{surf}/s_c(T_f)}$.

$$s_c(T_f) = \frac{A_{surf} \log e}{\log\left(\xi/k\tau_0\right)} \tag{6.11}$$

We compared to Ediger's experimental results using the linear representation for the configurational entropy, $s_c(T_f) = \Delta C_p(T_g^{bulk})(T_f - T_K)/T_K$. Along with A_{surf} obtained from equation 6.5, we take $\xi \approx 1nm$, $\tau_0 \sim 10^{-12}s$. $\Delta C_P(T_g^{bulk}) \approx 2.6k_B$ is the heat capacity jump at the glass transition for IMC in Boltzmann units per bead[24]. The theoretical results along with the measured values obtained by Ediger et al.[1] are plotted in figure 6.2. Our results are consistent with the experimental data for the deposition rates tested. The theory correctly predicts the trend for slower deposition rates. Despite the good agreement we point out that this is an approximate result in which we have assumed equilibrium relaxation, strictly true only for $T_{substrate} = T_f$.

It would seem natural to say that the enhanced mobility at the surface would penetrate into the bulk at least on the length scales of the bulk cooperative motion, as indeed it does. This however results in a local relaxation time $\tau_{local}(z)$ which changes by many orders of magnitude over just a few particle spacings. This mobility gradient would be relaxed via the dynamics of mode coupling theory, diffusing the excess mobility deeper into the bulk. In first approximation MCT has been shown to correlate dynamics on the length scale ξ_{MCT}[110], the predicted divergence of which at T_c will be broken by the emergence of activated events[181, 142]. A simple equation describing this smoothing of the mobility

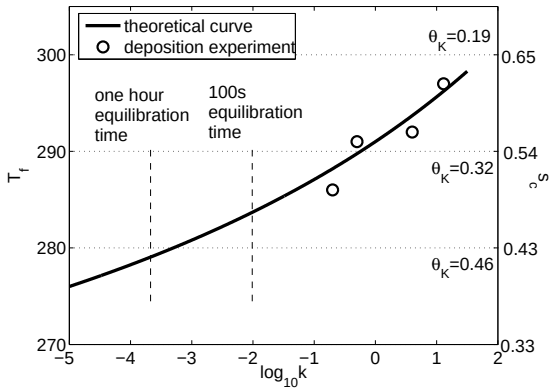

Figure 6.2: Fictive temperature vs deposition rate for the glass former IMC. Data for the deposition experiment was taken from reference [1]. Temperatures are converted into configurational entropy (right axis) and stability, θ_K, for comparison.

field, incorporating activated events in the framework of Bhattacharyya et al.[181] emerges

$$\xi_{MCT}^2 \nabla^2 \tau^{-1}(z) = \tau^{-1}(z) - \tau_{local}^{-1}(z). \tag{6.12}$$

If we treat the mobility profile from purely activated dynamics, $\tau_{local}^{-1}(z)$, as a set of boundary conditions at $z = 0$ and $z = \infty$ (equivalent to coarse graining on the length scale of the cooperative motion), then the mobility, decaying smoothly from $\tau_{surf}^{-1} \propto e^{-A_{surf}/s_c}$ on the free surface to $\tau_{bulk}^{-1} \propto e^{-A_{bulk}/s_c} \ll \tau_{surf}^{-1}$ in the bulk on a length scale ξ_{MCT}, would follow

$$\tau^{-1}(z) \approx \left(\tau_{surf}^{-1} - \tau_{bulk}^{-1}\right) e^{-z/\xi_{MCT}} + \tau_{bulk}^{-1}. \tag{6.13}$$

The distance the excess mobility penetrates, z^*, is found by comparing the magnitude of the two terms.

$$z^* = \xi_{MCT} \frac{A_{bulk} - A_{surf}}{s_c} \tag{6.14}$$

We have shown that $A_{surf} = \frac{1}{2} A_{bulk}$, and that $A_{bulk}/s_c(T_g) \approx 40$ at the glass transition. This gives a length scale $z^* \approx 20\xi_{MCT}$ which can be much larger than the bare dynamical correlation length.

At a depth $z < z^*$ from the surface the particle motion would freeze out when $\tau^{-1}(z) \approx e^{-A_{surf}/s_c(T_g^{local})} e^{-z/\xi_{MCT}} \approx \tau_{bulk}^{-1}(T_g)$, or when

$$\frac{A_{surf}}{s_c(T_g^{local})} + \frac{z}{\xi_{MCT}} = \frac{A_{bulk}}{s_c(T_g)} \tag{6.15}$$

We find that for the thinnest films local glass transition temperature will be $T_g^{min} = T_g^{surf}$ as expected. T_g^{local} will grow with distance from the free surface and be indistinguishable from the bulk at a depth z^*, on the order of 20nm in IMC.

The surface properties of glasses are important in many technological and biological contexts. Enhanced surface mobility is relevant for adhesion, friction, coatings, and nano-scale fabrication such as etching and lithography. Supercooled water at the surface of proteins acts to enslave many protein motions[182, 183]. Despite the influence of static surface perturbations, we feel that the idealized treatment of the surface mobility of glasses presented here can help in understanding these phenomena. The enhanced mobility at free surfaces will allow phase transformations to occur at the surface that are kinetically impossible in bulk. De-vitrification often occurs at free glass surfaces, a fact of some importance in geology[184] and archaeology[185]. This observation is naturally explained by the RFOT theory.

Chapter 6, in full, is a reprint of the material as it appears in the Journal of Chemical Physics 129 234514 (2008), J. D. Stevenson and P. G. Wolynes. The dissertation author was the primary investigator and author of this paper.

Bibliography

[1] Kearns, K. L. *et al.* Hiking down the energy landscape: Progress toward the Kauzmann temperature via vapor deposition. *J. Phys. Chem. B* **112**, 4934–4942 (2008).

[2] Simon, F. Über den zustand der unterkühlten flüssigkeiten und glässer. *Z. Anorg. Algemein. Chem.* **203**, 217 (1931).

[3] Kauzmann, W. The nature of the glassy state and the behavior of liquids at low temperatures. *Chemical Reviews* **43**, 219–256 (1948).

[4] Angell, C. A. Entropy and fragility in supercooling liquids. *NIST* **102**, 171–185 (1997).

[5] Adam, G. & Gibbs, J. H. On the temperature dependence of cooperative relaxation properties in glass-forming liquids. *J. Chem. Phys.* **43**, 139–146 (1965).

[6] Singh, Y., Stoessel, J. P. & Wolynes, P. G. Hard-sphere glass and the density-functional theory of aperiodic crystals. *Phys. Rev. Lett.* **54**, 1059–1062 (1985).

[7] Stoessel, J. P. & Wolynes, P. G. Linear excitations and the stability of the hard-sphere glass. *J. Chem. Phys.* **80**, 4502–4512 (1984).

[8] Gotze, W. & Sjogren, L. Relaxation processes in supercooled liquids. *Reports On Progress In Phys.* **55**, 241–376 (1992).

[9] Leutheusser, E. Dynamical model of the liquid-glass transition. *Phys. Rev. A* **29**, 2765–2773 (1984).

[10] Kirkpatrick, T. R. & Wolynes, P. G. Connections between some kinetic and equilibrium theories of the glass transition. *Phys. Rev. A* **35**, 3072–3080 (1987).

[11] Kirkpatrick, T. R. & Thirumalai, D. P-spin-interaction spin-glass models - connections with the structural glass problem. *Phys. Rev. B* **36**, 5388–5397 (1987).

[12] Crisanti, A. & Sommers, H. J. The spherical p-spin interaction spin-glass model - the statics. *Z. Fur Physik B: Cond. Matt.* **87**, 341–354 (1992).

[13] Castellani, T. & Cavagna, A. Spin-glass theory for pedestrians. *J. Stat. Mech. - Theory Exp.* P05012 (2005).

[14] Kirkpatrick, T. R. & Wolynes, P. G. Stable and metastable states in mean-field potts and structural glasses. *Phys. Rev. B* **36**, 8552–8564 (1987).

[15] Bouchaud, J. P. & Biroli, G. On the adam-gibbs-kirkpatrick-thirumalai-wolynes scenario for the viscosity increase in glasses. *J. Chem. Phys.* **121**, 7347–7354 (2004).

[16] Capaccioli, S., Ruocco, G. & Zamponi, F. Dynamically correlated regions and configurational entropy in supercooled liquids. *J. Phys. Chem. B* **112**, 10652–10658 (2008).

[17] Cammarota, C., Cavagna, A., Gradenigo, G., Grigera, T. S. & Verrocchio, P. Surface tension fluctuations and a new spinodal point in glass-forming liquids. *arXiv* (2009). `0904.1522`.

[18] Biroli, G., Bouchaud, J.-P., Cavagna, A., Grigera, T. S. & Verrocchio, P. Thermodynamic signature of growing amorphous order in glass-forming liquids. *Nature Phys.* **4**, 771–775 (2008).

[19] Kirkpatrick, T. R., Thirumalai, D. & Wolynes, P. G. Scaling concepts for the dynamics of viscous liquids near an ideal glassy state. *Phys. Rev. A* **40**, 1045–1054 (1989).

[20] Villain, J. Equilibrium critical properties of random field systems - new conjectures. *J. Physique* **46**, 1843–1852 (1985).

[21] Xia, X. & Wolynes, P. G. Fragilities of liquids predicted from the random first order transition theory of glasses. *Proc. Natl. Acad. Sci. U.S.A.* **97**, 2990–2994 (2000).

[22] Lubchenko, V. & Wolynes, P. G. Theory of aging in structural glasses. *J. Chem. Phys.* **121**, 2852–2865 (2004).

[23] Berthier, L. *et al.* Direct experimental evidence of a growing length scale accompanying the glass transition. *Science* **310**, 1797–1800 (2005).

[24] Stevenson, J. D. & Wolynes, P. G. Thermodynamic-kinetic correlations in supercooled liquids: A critical survey of experimental data and predictions of the random first-order transition theory of glasses. *J. Phys. Chem. B* **109**, 15093–15097 (2005).

[25] Böhmer, R., Ngai, K. L., Angell, C. A. & Plazek, D. J. Nonexponential relaxations in strong and fragile glass formers. *J. Chem. Phys.* **99**, 4201–4209 (1993).

[26] Kirkpatrick, T. R. & Thirumalai, D. Dynamics of the structural glass-transition and the p-spin-interaction spin-glass model. *Phys. Rev. Lett.* **58**, 2091–2094 (1987).

[27] Cugliandolo, L. F., Kurchan, J., Monasson, R. & Parisi, G. A mean-field hard-spheres model of glass. *J. Phys. A: Math. Gen.* **29**, 1347–1358 (1996).

[28] Mézard, M. & Parisi, G. Thermodynamics of glasses: A first principles computation. *Phys. Rev. Lett.* **82**, 747–750 (1999).

[29] Gross, D. J., Kanter, I. & Sompolinsky, H. Mean-field theory of the potts glass. *Phys. Rev. Lett.* **55**, 304–307 (1985).

[30] Gardner, E. Spin-glasses with p-spin interactions. *Nuclear Phys. B* **257**, 747–765 (1985).

[31] M. Mezard; G. Parisi, M. A. V. *Spin Glass Theory And Beyond* (World Scientific, Singapore, 1987).

[32] Biroli, G. & Mezard, M. Lattice glass models. *Phys. Rev. Lett.* **88**, 025501 (2002).

[33] Ciamarra, M. P., Tarzia, M., de Candia, A. & Coniglio, A. Lattice glass model with no tendency to crystallize. *Phys. Rev. E* **67**, 057105 (2003).

[34] Lopatin, A. V. & Ioffe, L. B. Structural glass on a lattice in the limit of infinite dimensions. *Phys. Rev. B* **66**, 174202 (2002).

[35] Schmalian, J. & Wolynes, P. G. Stripe glasses: Self-generated randomness in a uniformly frustrated system. *Phys. Rev. Lett.* **85**, 836–839 (2000).

[36] Anderson, P. W. *Basic Notions Of Condensed Matter Physics* (Westview Press, 1984).

[37] Chaikin, P. M. *Principles of Condensed Matter Physics* (Cambridge University Press, 1995).

[38] van Kampen, N. G. Condensation of classical gas with long-range attraction. *Phys. Rev. A: General Phys.* **135**, A362 (1964).

[39] Langer, J. S. Theory of condensation point. *Annals Phys.* **41**, 108 (1967).

[40] Maxwell, J. C. On the dynamical evidence of the molecular constitution of bodies–II. *Nature* **11**, 374–377 (1875).

[41] Maxwell, J. C. On the dynamical evidence of the molecular constitution of bodies. *Nature* **11**, 357–359 (1875).

[42] Sarkies, K. W. & Frankel, N. E. Nucleation theory with a nonclassical free energy. *J. Chem. Phys.* **54**, 433 (1971).

[43] Zel'Dovich, J. B. *Zh. Eksp. Teor. Fiz.* **12**, 525 (1942).

[44] Eastwood, M. P. & Wolynes, P. G. Droplets and the configurational entropy crisis for random first-order transitions. *Europhys. Lett.* **60**, 587–593 (2002).

[45] Lubchenko, V. & Wolynes, P. G. Barrier softening near the onset of nonactivated transport in supercooled liquids: Implications for establishing detailed connection between thermodynamic and kinetic anomalies in supercooled liquids. *J. Chem. Phys.* **119**, 9088–9105 (2003).

[46] Angell, C. A. Formation of glasses from liquids and biopolymers. *Science* **267**, 1924–1935 (1995).

[47] Wang, L. M. & Angell, C. A. Response to "Comment on 'Direct determination of the fragility indices of glassforming liquids by differential scanning calorimetry: Kinetic versus thermodynamic fragilities'" - [J. Chem. Phys. 118, 10351 (2003)]. *J. Chem. Phys.* **118**, 10353–10355 (2003).

[48] Brawer, S. A. Theory of relaxation in viscous-liquids and glasses. *J. Chem. Phys.* **81**, 954–975 (1984).

[49] Angell, C. A. & Smith, D. L. Test of the entropy basis of the vogel-tammann-fulcher equation - dielectric-relaxation of polyalcohols near tg. *J. Phys. Chem.* **86**, 3845–3852 (1982).

[50] Smith, D. L. Ph.D. thesis, Arizona State University, Arizona (1981).

[51] Naito, K. & Miura, A. Molecular design for nonpolymeric organic-dye glasses with thermal-stability - relations between thermodynamic parameters and amorphous properties. *J. Phys. Chem.* **97**, 6240–6248 (1993).

[52] Takahara, S., Yamamuro, O. & Suga, H. Heat-capacities and glass transitions of 1-propanol and 3-methylpentane under pressure - new evidence for the entropy theory. *J. Non Cryst. Sol.* **171**, 259–270 (1994).

[53] Moynihan, C. T. & Angell, C. A. Bond lattice or excitation model analysis of the configurational entropy of molecular liquids. *J. Non Cryst. Sol.* **274**, 131–138 (2000).

[54] Hikawa, H., Oguni, M. & Suga, H. Construction of an adiabatic calorimeter for a vapor-deposited sample and thermal characterization of amorphous butyronitrile. *J. Non. Cryst. Sol.* **101**, 90–100 (1988).

[55] Busch, R., Liu, W. & Johnson, W. L. Thermodynamics and kinetics of the Mg65Cu25Y10 bulk metallic glass forming liquid. *J. Appl. Phys.* **83**, 4134–4141 (1998).

[56] Takeda, K., Yamamuro, O., Tsukushi, I., Matsuo, T. & Suga, H. Calorimetric study of ethylene glycol and 1,3-propanediol: configurational entropy in supercooled polyalcohols. *J. Mol. Struct.* **479**, 227–235 (1999).

[57] Haida, O., Suga, H. & Seki, S. Calorimetric study of glassy state .12. plural glass-transition phenomena of ethanol. *J. Chem. Thermodynamics* **9**, 1133–1148 (1977).

[58] Alba-Simionesco, C., Fan, J. & Angell, C. A. Thermodynamic aspects of the glass transition phenomenon. II. Molecular liquids with variable interactions. *J. Chem. Phys.* **110**, 5262–5272 (1999).

[59] Wang, L. M., Velikov, V. & Angell, C. A. Direct determination of kinetic fragility indices of glassforming liquids by differential scanning calorimetry: Kinetic versus thermodynamic fragilities. *J. Chem. Phys.* **117**, 10184–10192 (2002).

[60] Richert, R. & Angell, C. A. Dynamics of glass-forming liquids. V. On the link between molecular dynamics and configurational entropy. *J. Chem. Phys.* **108**, 9016–9026 (1998).

[61] Wilde, G., Gorler, G. P., Willnecker, R. & Dietz, G. Thermodynamic properties of pd40ni40p20 in the glassy, liquid, and crystalline states. *Appl. Phys. Lett.* **65**, 397–399 (1994).

[62] Kawamura, Y. & Inoue, A. Newtonian viscosity of supercooled liquid in a Pd40Ni40P20 metallic glass. *Appl. Phys. Lett.* **77**, 1114–1116 (2000).

[63] Douslin, D. R. & Huffman, H. M. Low-temperature thermal data on the 5 isomeric hexanes. *J. Am. Chem. Soc.* **68**, 1704–1708 (1946).

[64] Yamamuro, O. *et al.* Calorimetric study of glassy and liquid toluene and ethylbenzene: Thermodynamic approach to spatial heterogeneity in glass-forming molecular liquids. *J. Phys. Chem. B* **102**, 1605–1609 (1998).

[65] Raemy, A. & Schweizer, T. F. Thermal-behavior of carbohydrates studied by heat-flow calorimetry. *J. Thermal Analysis* **28**, 95–108 (1983).

[66] Fan, J. Ph.D. thesis, Arizona State University, Arizona.

[67] Gangasharan, W. & Murthy, S. S. N. Nature of the relaxation processes in the supercooled liquid and glassy states of some carbohydrates. *J. Phys. Chem.* **99**, 12349–12354 (1995).

[68] Sanchez, E. M. Ph.D. thesis, Arizona State University, Arizona.

[69] Shamblin, S. L., Tang, X. L., Chang, L. Q., Hancock, B. C. & Pikal, M. J. Characterization of the time scales of molecular motion in pharmaceutically important glasses. *J. Phys. Chem. B* **103**, 4113–4121 (1999).

[70] Johari, G. P. Heat capacity and entropy of an equilibrium liquid from T-g to 0 K, and examining the conjectures of an underlying thermodynamic transition. *Chem. Phys.* **265**, 217–231 (2001).

[71] Mizukami, M., Fujimori, H. & Oguni, M. Glass transitions and the responsible molecular motions in 2-methyltetrahydrofuran. *Progress Theor. Phys. Supp.* **126**, 79–82 (1997).

[72] Crowley, K. J. & Zografi, G. The use of thermal methods for predicting glass-former fragility. *Thermochimica Acta* **380**, 79–93 (2001).

[73] Hancock, B. C. & Parks, M. What is the true solubility advantage for amorphous pharmaceuticals? *Pharm. Res.* **17**, 397–404 (2000).

[74] Aso, Y., Yoshioka, S. & Kojima, S. Relationship between the crystallization rates of amorphous nifedipine, phenobarbital, and flopropione, and their molecular mobility as measured by their enthalpy relaxation and H-1 NMR relaxation times. *J. Pharm. Sci.* **89**, 408–416 (2000).

[75] Plazek, D. J. & Magill, J. H. Physical properties of aromatic hydrocarbons .i. viscoelastic behavior of 1.3.5-tri-alpha-naphthyl benzene. *J. Chem. Phys.* **45**, 3038 (1966).

[76] Magill, J. H. Physical properties of aromatic hydrocarbons .3. a test of Adam-Gibbs relaxation model for glass formers based on heat-capacity data of 1,3,5-tri-alpha-naphthylbenzene. *J. Chem. Phys.* **47**, 2802 (1967).

[77] Tsukushi, I. *et al.* A calorimetric study on the configurational enthalpy and low-energy excitation of ground amorphous solid and liquid-quenched glass of 1,3,5-tri-alpha-naphthylbenzene. *J. Phys.: Cond. Matt.* **8**, 245–255 (1996).

[78] Johari, G. P. An equilibrium supercooled liquid's entropy and enthalpy in the Kauzmann and the third law extrapolations, and a proposed experimental resolution. *J. Chem. Phys.* **113**, 751–761 (2000).

[79] Takahara, S., Yamamuro, O. & Matsuo, T. Calorimetric study of 3-bromopentane: Correlation between structural relaxation time and configurational entropy. *J. Phys. Chem.* **99**, 9589–9592 (1995).

[80] Lebrun, N. & van Miltenburg, J. C. Calorimetric study of maltitol: correlation between fragility and thermodynamic properties. *J. Alloys Compounds* **320**, 320–325 (2001).

[81] Faivre, A. *et al.* Dynamics of sorbitol and maltitol over a wide time-temperature range. *Euro. Phys. J. B* **10**, 277–286 (1999).

[82] Carpentier, L., Bourgeois, L. & Descamps, M. Contribution of temperature modulated DSC (R) to the study of the molecular mobility in glass forming pharmaceutical systems. *J. Therm. Anal. Calor.* **68**, 727–739 (2002).

[83] Meva'a, L. M. & Lichanot, A. Proprits thermodynamiques en phase condense des ortho, mta et para fluorotolune, crsol et toluidine. *Thermochimica Acta* **158**, 335–345 (1990).

[84] Cutroni, M., Mandanici, A., Spanoudaki, A. & Pelster, R. The alpha-relaxation process in simple glass forming liquid m-toluidine. I. The temperature dependence of the dielectric response. *J. Chem. Phys.* **114**, 7118–7123 (2001).

[85] Murthy, S. S. N., Paikaray, A. & Arya, N. Molecular relaxation and excess entropy in liquids and their connection to the structure of glass. *J. Chem. Phys.* **102**, 8213–8220 (1995).

[86] Hikima, T., Okamoto, N., Hanaya, M. & Oguni, M. Calorimetric study of triphenylethene: observation of homogeneous-nucleation-based crystallization. *J. Chem. Thermod.* **30**, 509–523 (1998).

[87] Hikima, T., Hanaya, M. & Oguni, M. Microscopic observation of a peculiar crystallization in the glass transition region and beta-process as potentially controlling the growth rate in triphenylethylene. *J. Mol. Struct.* **479**, 245–250 (1999).

[88] Nozaki, R., Suzuki, D., Ozawa, S. & Shiozaki, Y. The alpha and the beta relaxation processes in supercooled sorbitol. *J. Non Cryst. Sol.* **235**, 393–398 (1998).

[89] Kunzler, J. E. & Giauque, W. F. The heat capacity and entropy of sulfuric acid trihydrate glass and crystals from 15-degrees-k to 300-degrees-k. *J. Am. Chem. Soc.* **74**, 797–800 (1952).

[90] Fujimori, H. & Oguni, M. Calorimetric study of d,l-propene carbonate - observation of the beta-glass as well as alpha-glass transition in the supercooled liquid. *J. Chem. Thermodynamics* **26**, 367–378 (1994).

[91] Angell, C. A., Boehm, L., Oguni, M. & Smith, D. L. Far ir-spectra and heat-capacities for propylene carbonate and propylene-glycol, and the connection to the dielectric response function. *J. Mol. Liq.* **56**, 275–286 (1993).

[92] Jackson, C. L. & Mckenna, G. B. The melting behavior of organic materials confined in porous solids. *J. Chem. Phys.* **93**, 9002–9011 (1990).

[93] Dzero, M., Schmalian, J. & Wolynes, P. G. Activated events in glasses: The structure of entropic droplets. *Phys. Rev. B* **72**, 100201 (2005).

[94] Huang, D. H. & McKenna, G. B. New insights into the fragility dilemma in liquids. *J. Chem. Phys.* **114**, 5621–5630 (2001).

[95] Biroli, G., Bouchaud, J. P. & Tarjus, G. Are defect models consistent with the entropy and specific heat of glass formers? *J. Chem. Phys.* **123**, 044510 (2005).

[96] Franz, S. & Toninelli, F. L. A field-theoretical approach to the spin glass transition: models with long but finite interaction range. *J. Stat. Mech: Thoer. and Exp.* P01008 (2005).

[97] Franz, S. Metastable states, relaxation times and free-energy barriers in finite-dimensional glassy systems. *Europhys. Lett.* **73**, 492–498 (2006).

[98] Xia, X. & Wolynes, P. G. Microscopic theory of heterogeneity and nonexponential relaxations in supercooled liquids. *Phys. Rev. Lett.* **86**, 5526–5529 (2001).

[99] Ediger, M. D. Spatially heterogeneous dynamics in supercooled liquids. *Ann. Rev. Phys. Chem.* **51**, 99–128 (2000).

[100] Russell, E. V. & Israeloff, N. E. Direct observation of molecular cooperativity near the glass transition. *Nature* **408**, 695–698 (2000).

[101] Deschenes, L. A. & Bout, D. A. V. Single-molecule studies of heterogeneous dynamics in polymer melts near the glass transition. *Science* **292**, 255–258 (2001).

[102] Sillescu, H. Heterogeneity at the glass transition: a review. *J. Non-Cryst. Solids* **243**, 81–108 (1999).

[103] Richert, R. Heterogeneous dynamics in liquids: fluctuations in space and time. *J. Phys.: Cond. Matt.* **24**, R703–R738 (2002).

[104] Kob, W., Donati, C., Plimpton, S. J., Poole, P. H. & Glotzer, S. C. Dynamical heterogeneities in a supercooled lennard-jones liquid. *Phys. Rev. Lett.* **79**, 2827–2830 (1997).

[105] Gebremichael, Y., Vogel, M. & Glotzer, S. C. Particle dynamics and the development of string-like motion in a simulated monoatomic supercooled liquid. *J. Chem. Phys.* **120**, 4415–4427 (2004).

[106] Donati, C. *et al.* Stringlike cooperative motion in a supercooled liquid. *Phys. Rev. Lett.* **80**, 2338–2341 (1998).

[107] Donati, C., Glotzer, S. C., Poole, P. H., Kob, W. & Plimpton, S. J. Spatial correlations of mobility and immobility in a glass-forming lennard-jones liquid. *Phys. Rev. E* **60**, 3107–3119 (1999).

[108] Weeks, E. R., Crocker, J. C., Levitt, A. C., Schofield, A. & Weitz, D. A. Three-dimensional direct imaging of structural relaxation near the colloidal glass transition. *Science* **287**, 627–631 (2000).

[109] Reinsberg, S. A., Heuer, A., Doliwa, B., Zimmermann, H. & Spiess, H. W. Comparative study of the nmr length scale of dynamic heterogeneities of three different glass formers. *J. Non-Cryst. Solids* **307–310**, 208–214 (2002).

[110] Biroli, G. & Bouchaud, J. P. Diverging length scale and upper critical dimension in the Mode-Coupling Theory of the glass transition. *Europhys. Lett.* **67**, 21–27 (2004).

[111] Unger, C. & Klein, W. Nucleation theory near the classical spinodal. *Phys. Rev. B* **29**, 2698–2708 (1984).

[112] Johnson, G., Mel'cuk, A. I., Gould, H., Klein, W. & Mountain, R. D. Molecular-dynamics study of long-lived structures in a fragile glass-forming liquid. *Phys. Rev. E* **57**, 5707–5718 (1998).

[113] Dasgupta, C. & Valls, O. T. Free energy landscape of a dense hard-sphere system. *Phys. Rev. E* **59**, 3123–3134 (1999).

[114] Fuchizaki, K. & Kawasaki, K. Dynamical density functional theory for glassy behaviour. *J. Phys.: Cond. Matt.* **14**, 12203–12222 (2002).

[115] Stillinger, F. H. & Weber, T. A. Dynamics of structural transitions in liquids. *Phys. Rev. A* **28**, 2408–2416 (1983).

[116] Hall, R. W. & Wolynes, P. G. Microscopic theory of network glasses. *Phys. Rev. Lett.* **90**, 085505 (2003).

[117] Stauffer, D. Monte-carlo study of density profile, radius, and perimeter for percolation clusters and lattice animals. *Phys. Rev. Lett.* **41**, 1333–1336 (1978).

[118] Leath, P. L. Cluster size and boundary distribution near percolation threshold. *Phys. Rev. B* **14**, 5046–5055 (1976).

[119] Yang, C. N. & Lee, T. D. Statistical theory of equations of state and phase transitions. i. theory of condensation. *Phys. Rev.* **87**, 404–409 (1952).

[120] Sykes, M. F., Gaunt, D. S. & Glen, M. Percolation processes in three dimensions. *J. Phys. A: Math. Gen.* **9**, 1705–1712 (1976).

[121] Cao, Q. Z. & Wong, P. O. External surface of site percolation clusters in three dimensions. *J. Phys. A: Math. Gen.* **25**, L69–L74 (1992).

[122] Stickel, F., Fischer, E. W. & Richert, R. Dynamics of glass-forming liquids .2. detailed comparison of dielectric relaxation, dc-conductivity, and viscosity data. *J. Chem. Phys.* **104**, 2043–2055 (1996).

[123] Novikov, V. N. & Sokolov, A. P. Universality of the dynamic crossover in glass-forming liquids: A "magic" relaxation time. *Phys. Rev. E* **67**, 031507 (2003).

[124] Chui, S. T. & Weeks, J. D. Phase-transition in 2-dimensional coulomb gas, and interfacial roughening transition. *Phys. Rev. B* **14**, 4976–4982 (1976).

[125] Böhmer, R. & Angell, C. A. Correlations of the nonexponentiality and state dependence of mechanical relaxations with bond connectivity in Ge-As-Se supercooled liquids. *Phys. Rev. B* **45**, 10091–10094 (1992).

[126] Laughlin, W. T. & Uhlmann, D. R. Viscous flow in simple organic liquids. *J. Phys. Chem* **76**, 2317–2325 (1972).

[127] Cukierman, M., Lane, J. W. & Uhlmann, D. R. High-temperature flow behavior of glass-forming liquids: A free-volume interpretation. *J. Chem. Phys.* **59**, 3639–3644 (1973).

[128] Hinze, G., Brace, D. D., Gottke, S. D. & Fayer, M. D. A detailed test of mode-coupling theory on all time scales: Time domain studies of structural relaxation in a supercooled liquid. *J. Chem. Phys.* **113**, 3723–3733 (2000).

[129] Flory, P. J. *Principles of Polymer Chemistry* (Cornell University Press Ltd., 1953).

[130] Tracht, U. *et al.* Length scale of dynamic heterogeneities at the glass transition determined by multidimensional nuclear magnetic resonance. *Phys. Rev. Lett.* **81**, 2727–2730 (1998).

[131] Adichtchev, S. *et al.* Fast relaxation processes in glasses as revealed by depolarized light scattering. *Journal of Non-Crystalline Solids* **353**, 1491–1500 (2007).

[132] Kudlik, A., Benkhof, S., Blochowicz, T., Tschirwitz, C. & Rossler, E. The dielectric response of simple organic glass formers. *J. Mol. Struct.* **479**, 201–218 (1999).

[133] Ngai, K. L. & Capaccioli, S. Relation between the activation energy of the Johari-Goldstein β relaxation and T_g of glass formers. *Phys. Rev. E* **69**, 031501 (2004).

[134] Wang, L. M. & Richert, R. Primary and secondary relaxation time dispersions in fragile supercooled liquids. *Phys. Rev. B* **76**, 064201 (2007).

[135] Lunkenheimer, P., Schneider, U., Brand, R. & Loidl, A. Glassy dynamics. *Contemporary Phys.* **41**, 15–36 (2000).

[136] Frauenfelder, H. *et al.* A unified model of protein dynamics. *Proc. Natl. Acad. Sci. U.S.A.* (2009).

[137] Thayyil, M. S., Capaccioli, S., Prevosto, D. & Ngai, K. L. Is the Johari-Goldstein beta-relaxation universal? *Philosophical Magazine* **88**, 4007–4013 (2008).

[138] Lubchenko, V. & Wolynes, P. G. Theory of structural glasses and supercooled liquids. *Ann. Rev. Phys. Chem.* **58**, 235–266 (2007).

[139] Dzero, M., Schmalian, J. & Wolynes, P. G. Replica theory for fluctuations of the activation barriers in glassy systems. *arXiv:0809.3988v1* (2008).

[140] Stevenson, J. D., Schmalian, J. & Wolynes, P. G. The shapes of cooperatively rearranging regions in glass-forming liquids. *Nature Phys.* **2**, 268–274 (2006).

[141] Stevenson, J. D., Walczak, A. M., Hall, R. W. & Wolynes, P. G. Constructing explicit magnetic analogies for the dynamics of glass forming liquids. *J. Chem. Phys.* **129**, 194505 (2008).

[142] Bhattacharyya, S. M., Bagchi, B. & Wolynes, P. G. Facilitation, complexity growth, mode coupling, and activated dynamics in supercooled liquids. *Proc. Natl. Acad. Sci. U.S.A.* **105**, 16077–16082 (2008).

[143] Hagedorn, R. Statistical thermodynamics of strong interactions at high-energies. *Nuovo Cim. Suppl.* **3**, 147 (1965).

[144] Plotkin, S. S. & Wolynes, P. G. Buffed energy landscapes: Another solution to the kinetic paradoxes of protein folding. *Proc. Natl. Acad. Sci. U.S.A.* **100**, 4417–4422 (2003).

[145] Wiedersich, J. *et al.* Fast and slow relaxation processes in glasses. *J. Phys.: Cond. Matt.* **11**, A147–A156 (1999).

[146] Mezard, M. & Parisi, G. Statistical physics of structural glasses. *J. Phys.: Cond. Matt.* **12**, 6655–6673 (2000).

[147] Bertin, E. Global fluctuations and gumbel statistics. *Phys. Rev. Lett.* **95**, 170601 (2005).

[148] Blochowicz, T., Tschirwitz, C., Benkhof, S. & Rossler, E. A. Susceptibility functions for slow relaxation processes in supercooled liquids and the search for universal relaxation patterns. *J. Chem. Phys.* **118**, 7544–7555 (2003).

[149] Blochowicz, T., Gainaru, C., Medick, P., Tschirwitz, C. & Rossler, E. A. The dynamic susceptibility in glass forming molecular liquids: The search for universal relaxation patterns II. *J. Chem. Phys.* **124**, 134503 (2006).

[150] Das, S. P. Mode-coupling theory and the glass transition in supercooled liquids. *Rev. Modern Phys.* **76**, 785–851 (2004).

[151] Young, A. P. (ed.) *Spin glasses and random fields* (World Scientific Publishing Co. Pte. Ltd., 1997).

[152] Marinari, E., Parisi, G., Ricci-Tersenghi, F., Ruiz-Lorenzo, J. J. & Zuliani, F. Replica symmetry breaking in short-range spin glasses: Theoretical foundations and numerical evidences. *J. Stat. Phys.* **98**, 973–1047 (2000).

[153] Parisi, G. Spin glass theory: Numerical and experimental results in three-dimensional systems. *Physica A* **386**, 611–624 (2007).

[154] Huse, D. & Fisher, D. S. Dynamics of droplet fluctuations in pure and random ising systems. *Phys. Rev. B* **35**, 6841–6846 (1987).

[155] Mcmillan, W. L. Domain-wall renormalization-group study of the 3-dimensional random ising-model at finite temperature. *Phys. Rev. B* **31**, 340–341 (1985).

[156] Huse, D. & Fisher, D. S. On the behavior of ising spin-glasses in a uniform magnetic-field. *J. Phys. I* **1**, 621–625 (1991).

[157] Franz, S. & Parisi, G. Recipes for metastable states in spin-glasses. *J. Phys. I* **5**, 1401–1415 (1995).

[158] Tarzia, M. & Moore, M. A. Glass phenomenology from the connection to spin glasses. *Phys. Rev. E* **75**, 031502 (2007).

[159] Temesvári, T. Almeida-thouless transition below six dimensions. *Phys. Rev. B* **78**, 220401 (2008).

[160] Stillinger, F. H., Debenedetti, P. G. & Truskett, T. M. The Kauzmann paradox revisited. *J. Phys. Chem. B* **105**, 11809–11816 (2001).

[161] Monasson, R. Structural glass-transition and the entropy of the metastable states. *Phys. Rev. Lett.* **75**, 2847–2850 (1995).

[162] Fixman, M. Highly anharmonic crystal. *J. Chem. Phys.* **51**, 3270 (1969).

[163] Hall, R. W. & Wolynes, P. G. Intermolecular forces and the glass transition. *J. Phys. Chem. B* **112**, 301–312 (2008).

[164] Migliorini, G. & Berker, A. N. Global random-field spin-glass phase diagrams in two and three dimensions. *Phys. Rev. B* **57**, 426–431 (1998).

[165] Kob, W. & Andersen, H. C. Scaling behavior in the beta-relaxation regime of a supercooled lennard-jones mixture. *Phys. Rev. Lett.* **73**, 1376–1379 (1994).

[166] Landau, L. D. & Lifshitz, E. M. *Statistical Physics* (Addison–Wesley, Reading, MA, 1969).

[167] Ferrenberg, A. M. & Swendsen, R. H. New monte-carlo technique for studying phase-transitions. *Phys. Rev. Lett.* **61**, 2635–2638 (1988).

[168] Ferrenberg, A. M. & Swendsen, R. H. Optimized monte-carlo data-analysis. *Phys. Rev. Lett.* **63**, 1195–1198 (1989).

[169] Drozdov, A. N., Grossfield, A. & Pappu, R. V. Role of solvent in determining conformational preferences of alanine dipeptide in water. *J. Am. Chem. Soc.* **126**, 2574–2581 (2004).

[170] Cammarota, C. & Cavagna, A. A novel method for evaluating the critical nucleus and the surface tension in systems with first order phase transition. *J. Chem. Phys.* **127**, 214703 (2007).

[171] Rowlinson, J. S. & Widom, B. *Molecular theory of capillarity* (Oxford University Press, New York, 1982).

[172] Swallen, S. F. *et al.* Organic glasses with exceptional thermodynamic and kinetic stability. *Science* **315**, 353–356 (2007).

[173] Fakhraai, Z. & Forrest, J. A. Measuring the surface dynamics of glassy polymers. *Science* **319**, 600–604 (2008).

[174] Kivelson, D., Kivelson, S. A., Zhao, X. L., Nussinov, Z. & Tarjus, G. A thermodynamic theory of supercooled liquids. *Physica A* **219**, 27–38 (1995).

[175] Franz, S. & Parisi, G. On non-linear susceptibility in supercooled liquids. *J. Phys.: Cond. Matt.* **12**, 6335–6342 (2000).

[176] Alcoutlabi, M. & Mckenna, G. B. Effects of confinement on material behaviour at the nanometre size scale. *J. Phys.: Cond. Matt.* **17**, R461–R524 (2005).

[177] Forrest, J. A., Dalnokiveress, K., Stevens, J. R. & Dutcher, J. R. Effect of free surfaces on the glass transition temperature of thin polymer films. *Phys. Rev. Lett.* **77**, 2002–2005 (1996).

[178] Li, C. H. *et al.* Viscosity measurements of very thin polymer films. *Macromolecules* **38**, 5144–5151 (2005).

[179] Zhang, J., Liu, G. & Jonas, J. Effects of confinement on the glass-transition temperature of molecular liquids. *J. Phys. Chem.* **96**, 3478–3480 (1992).

[180] Franz, S. & Montanari, A. Analytic determination of dynamical and mosaic length scales in a Kac glass model. *J. Phys. A: Math. Theor.* **40**, F251–F257 (2007).

[181] Bhattacharyya, S. M., Bagchi, B. & Wolynes, P. G. Bridging the gap between the mode coupling and the random first order transition theories of structural relaxation in liquids. *Phys. Rev. E* **72**, 031509 (2005).

[182] Lubchenko, V., Wolynes, P. G. & Frauenfelder, H. Mosaic energy landscapes of liquids and the control of protein conformational dynamics by glass-forming solvents. *J. Phys. Chem. B* **109**, 7488–7499 (2005).

[183] Frauenfelder, H., Sligar, S. G. & Wolynes, P. G. The energy landscapes and motions of proteins. *Science* **254**, 1598–1603 (1991).

[184] Marshall, R. R. Devitrification of natural glass. *Geological Society of America Bulletin* **72**, 1493–1520 (1961).

[185] Richards, W. T. Remarks concerning the formation and crystallization of vitreous media. *J. Chem. Phys.* **4**, 449–457 (1936).